Tectonophysics 671 (2016) 218–234

Contents lists available at ScienceDirect

Tectonophysics

journal homepage: www.elsevier.com/locate/tecto

Pre-collisional accretionary growth of the southern Laurasian active margin, Central Pontides, Turkey

Mesut Aygül [a,b,*], Aral I. Okay [a], Roland Oberhänsli [b], Masafumi Sudo [b]

[a] İstanbul Technical University, Eurasia Institute of Earth Sciences, 34469, Maslak, İstanbul, Turkey
[b] University of Potsdam, Institute of Earth and Environmental Science, Karl-Liebknecht-Str. 24–25, 14476 Potsdam-Golm, Germany

ARTICLE INFO

Article history:
Received 16 February 2015
Received in revised form 3 October 2015
Accepted 4 January 2016
Available online 27 January 2016

Keywords:
Laurasian margin
Accretionary growth
Subduction–accretionary complexes
HP/LT metamorphism
Blueschists

ABSTRACT

Cretaceous subduction–accretionary complexes crop out over wide areas in the central part of the Pontides, northern Turkey. To the north, the wedge consists of a low-grade metaflysch sequence with blocks of marble, Na-amphibole-bearing metabasite (PT = 7–12 kbar; 400 ± 70 °C) and serpentinite. $^{40}Ar/^{39}Ar$ phengite ages from the phyllites of the metaflysch are ca. 100 Ma. The metaflysch sequence is underlain by oceanic crust-derived *HP/LT* metabasites and micaschists along a major detachment fault. The metabasites are epidote-blueschists consisting of glaucophane, epidote, titanite, and phengite locally with garnet. Fresh lawsonite-blueschists are exposed as blocks along the detachment fault. Peak metamorphic conditions of a garnet-blueschist are constrained to 17 ± 1 kbar and 500 ± 40 °C and of a lawsonite-blueschist to 14 ± 2 kbar and 370–440 °C. $^{40}Ar/^{39}Ar$ phengite dating on the micaschists constrains the *HP/LT* metamorphism as 101–92 Ma, younging southward. Middle Jurassic (ca. 160 Ma) accretionary complexes consisting of blueschist to lower greenschist facies metabasites, marble and volcanogenic metasediment intercalations are exposed at the southern part of the Cretaceous wedge. In the studied area, the North Anatolian Fault forms the contact between Cretaceous and Middle Jurassic *HP/LT* metamorphic rocks. Wide distribution of Cretaceous subduction–accretionary complexes implies accretionary tectonic continental growth along the Laurasian active margin. High amount of clastic sediment flux into the trench has a major effect on enlarging the wedge during the Albian. Tectonic thickening of the oceanic *HP/LT* metamorphic sequence, however, was possibly achieved by propagation of the décollement along the retreating slab which can create the space necessary for progressive deep level basal underplating and extension of the wedge for subsequent syn-subduction exhumation.

1. Introduction

Accretionary, Pacific- or Turkic-type orogenies have been used to emphasize the importance of pre-collisional history of subduction and accretion processes in creating new continental crust (Cawood et al., 2009; Dickinson, 2008; Maruyama, 1997; Şengör and Natal'in, 1996; Şengör et al., 1993). This includes addition of juvenile material to the crust in the magmatic arcs and tectonic growth of the associated accretionary prism towards subduction. Additionally, oceanic crustal edifices like seamounts, oceanic plateaus and intra oceanic arcs are favored to accrete rather than recycled into the mantle due to their relatively high buoyancy (Cloos, 1993). An accretionary prism is recognized by tectonically thickened subduction–accretionary complexes composed of trench turbidites, high pressure/low temperature (*HP/LT*) metamorphic rocks, ophiolitic fragments and mélanges. Two modes of accretion are proposed: i) frontal accretion through scraping off mainly trench-fill turbidites and oceanic pelagic sediments as wedge shaped packages (e.g. Karig and Sharman, 1975; Moore et al., 1982; Seely et al., 1974; Ujiee, 1997) and ii) underplating as duplexes beneath the offscraped part of the prism (e.g. Kimura et al., 1996; Moore et al., 1991; Sample and Fisher, 1986; Platt et al., 1985). A significant portion of accretion occurs at deeper parts of the accretionary wedge evidenced by eclogite and blueschist facies metamorphic rocks of the exhumed subduction–accretionary complexes (e.g. Agard et al., 2001; Barr et al., 1999; Okay et al., 2006a, 2002; Takasu et al., 1994; Tsujimori et al., 2006a). Tectonic thickening of these deep-seated *HP/LT* metamorphic rocks, however, remains ambiguous due to the necessary space problem for basal accretion along the plate interface.

Accretionary orogenies have been defined in many regions including the Altaids (Şengör and Natal'in, 1996; Şengör et al., 1993), the Circum-Pacific realm (e.g. Dickinson, 2008; Fuis et al., 2008; Isozaki, 1996; Maruyama, 1997), and the Lachlan orogeny of eastern Australia (Foster and Gray, 2000; Spaggiari et al., 2002). In contrast, in the Alpine–Himalayan orogenic belt, accretionary complexes or mélanges associated with closure of the former Tethys Ocean are generally interpreted in terms of sutures separating the continental blocks or

* Corresponding author at: İTU Ayazağa Kampüsü, Avrasya Yer Bilimleri Enstitüsü, 34469 Maslak, İstanbul, Turkey.
E-mail address: aygulm@itu.edu.tr (M. Aygül).

http://dx.doi.org/10.1016/j.tecto.2016.01.010
0040-1951/

terranes (Şengör and Natal'in, 1996). In the Anatolian scale, Şengör and Yilmaz (1981) interpreted Eastern Anatolia as a large accretionary complex based on scarce occurrences of Late Cretaceous ophiolitic mélanges and flysch.

In this study, we describe a new accretionary-type orogenic area in the central part of the Pontides, northern Turkey; a mountain chain within the Alpine–Himalayan orogenic belt. In the Central Pontides, Middle Jurassic and Cretaceous subduction–accretionary complexes called the Central Pontide Supercomplex (CPS) extend over large areas (Okay et al., 2013). In the CPS, Cretaceous accretionary complexes consist of *HP/LT* metamorphic units of continental and oceanic origin as well as mélanges representing the Laurasian active continental margin. The continental accretionary rocks are represented by distal turbidites of low metamorphic grade exposed to the north. They are underlain by oceanic crust derived deep-seated *HP/LT* metamorphic rocks along a detachment fault. Middle Jurassic subduction–accretionary complexes are exposed within the Cretaceous accretionary wedge as tectonic slices. Here, we present new petrologic, geochronological and structural data and a new geological map along a north–south section in order to unravel the tectonic evolution of the Mesozoic accretionary complexes in the Central Pontides. A second aim of the paper is to discuss the mechanism of the tectonic thickening of the deep-seated *HP/LT* metamorphic sequences.

2. Geological setting

The Pontides are the mountain chain between the Black Sea and the İzmir–Ankara–Erzincan suture (Fig. 1). Before the Late Cretaceous opening of the Black Sea as a back-arc basin (e.g. Okay et al., 2013, 1994), the Pontides constituted part of the continental margin of Laurasia. The Pontides are divided into three tectonic units: the Strandja Massif, the İstanbul and Sakarya zones (Okay, 1989; Fig. 1). Contact relations between these tectonic units are still controversial. However, the most prominent structure is the east–west striking Intra-Pontide suture, separating the İstanbul Zone from the Sakarya Zone (Akbayram et al., 2013; Göncüoglu et al., 2014; Okay and Tüysüz, 1999; Robertson and Ustaömer, 2004).

In the Central Pontides (Fig. 2), the İstanbul Zone is represented by a Neo-Proterozoic crystalline basement consisting of tonalitic and granitic metagranitoids with 590–560 Ma zircon crystallization ages (Chen et al., 2002), similar to other upper Neoproterozoic granitoids from the basement of the İstanbul Zone (Ustaömer and Rogers, 1999; Ustaömer et al., 2005; Yiğitbaş et al., 2004). The basement rocks are stratigraphically overlain by Early Ordovician to Devonian sedimentary rocks of the İstanbul Paleozoic sequence (Boztuğ, 1992; Dean et al., 2000). Okay et al. (1994) suggest that İstanbul Zone was rifted from the Moesian Platform to the north during opening of the Black Sea.

The Sakarya Zone forms a ribbon along northern Turkey, consisting of slivers of Devonian granitoids (Aysal et al., 2012; Okay et al., 1996; Sunal, 2012), Permo-Carboniferous high-grade metamorphic and related intrusive rocks (Okay et al., 2006b, 1996; Topuz et al., 2007, 2004), and Late Triassic subduction–accretionary complexes with eclogite and blueschist slices (Okay, 2000; Okay and Okay and Monié, 1997; Okay et al., 2002; Pickett and Robertson, 2004; Robertson and Ustaömer, 2012; Topuz et al., 2014). Recently, Middle Jurassic subduction–accretionary complexes were also reported in the Eastern Pontides suggesting an episodic accretionary construction of the Pontides (Topuz et al., 2012). In the Central Pontides, the Sakarya Zone consists of Permo-Carboniferous granitic rocks (Nzegge et al., 2006; Okay et al., 2015) and Upper Triassic turbidites with dismembered ophiolitic rocks, known as the Küre Complex, (Okay et al., 2015; Ustaömer and Robertson, 1997, 1994, 1993). The Küre Complex is intruded by Middle Jurassic granitoids representing part of a major magmatic arc (Okay et al., 2014; Yılmaz and Boztuğ, 1986). The granitoids are associated with Middle Jurassic low pressure and high temperature metamorphic rocks constituting deeper levels of the magmatic arc (Okay et al., 2014).

Upper Jurassic limestones and Lower Cretaceous turbidites unconformably cover the rocks of İstanbul and Sakarya zones (Hippolyte

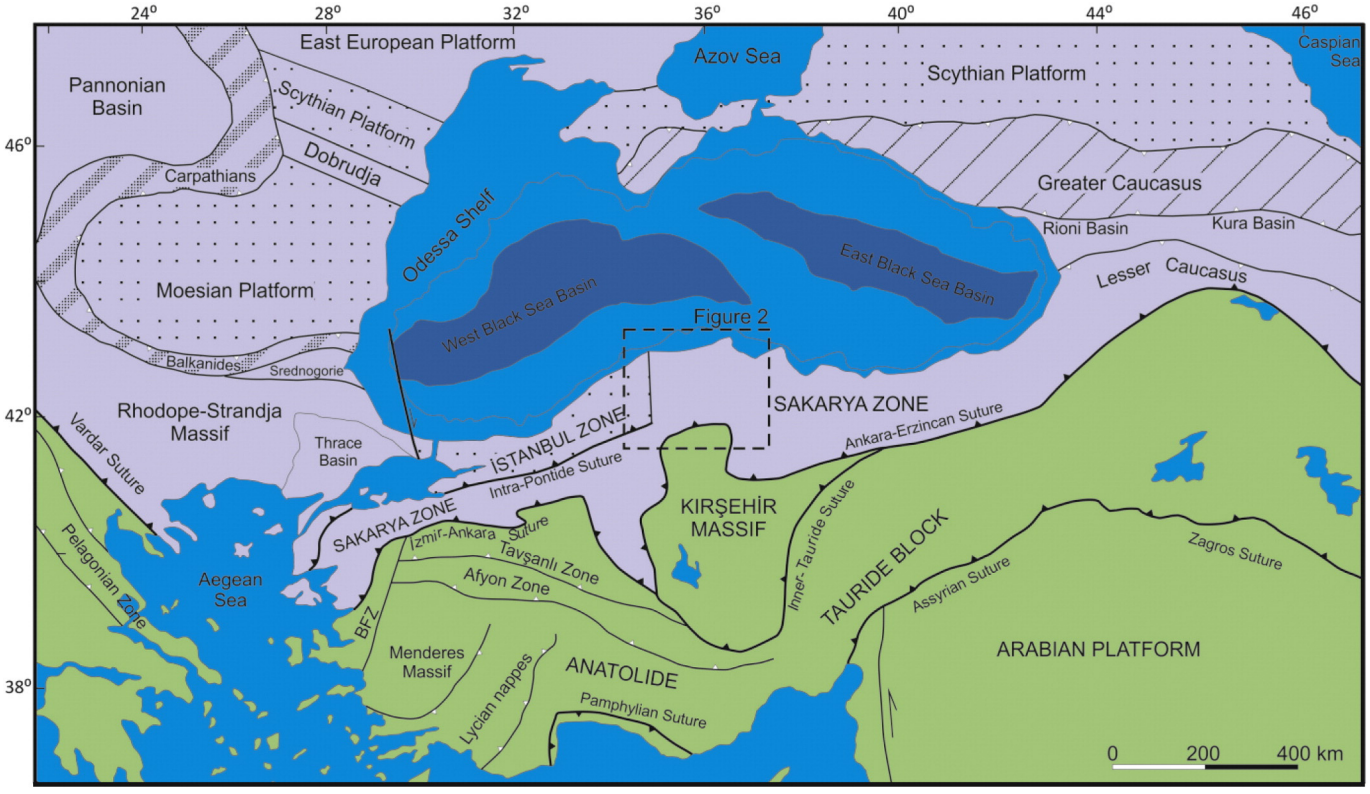

Fig. 1. Tectonic map of Turkey and surrounding regions. Modified from Okay and Tüysüz (1999). East–West trending İzmir–Ankara–Erzincan suture separates tectonic units with Mesozoic Laurasian (purple) and with Gondwanan (green) affinities.

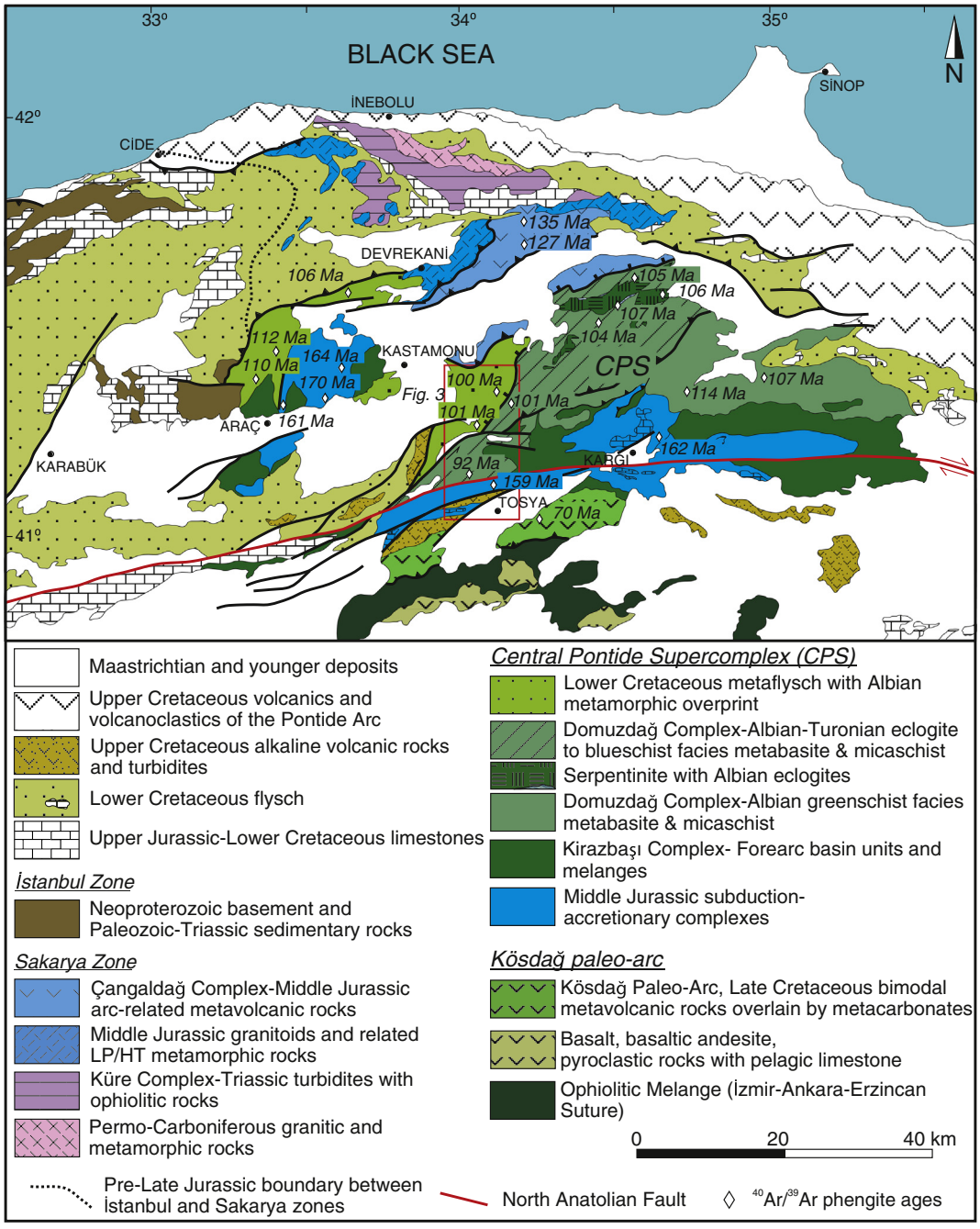

Fig. 2. Geological map of the Central Pontides. Base map is from Uğuz et al. (2002). Central Pontide Supercomplex is modified from Okay et al. (2014, 2013), Tüysüz (1990) and this study.

et al., 2010; Okay et al., 2013; Tüysüz, 1999), indicating that these tectonic zones were juxtaposed before the Late Jurassic. The Lower Cretaceous turbidites represent a large submarine fan and detrital zircons indicate a major source area in the East European Craton and Scythian Platform north of the Black Sea, showing that the opening of the Black Sea basin took place after Early Cretaceous time (Okay et al., 2013). This is also documented by Turonian–Campanian volcano-sedimentary successions interlayered with deep marine sedimentary rocks representing the opening of the Black Sea as a back-/intra-arc basin (Tüysüz et al., 2015, 2012).

South of the Lower Cretaceous turbidites, metamorphic rocks of mostly *HP/LT* in origin crop out over a large area. The *HP/LT* metamorphic rocks are generally assumed to be of Triassic age and placed in a key role in Paleo- and Neo-Tethyan reconstructions of Turkey (e.g. Tüysüz, 1990; Ustaömer and Robertson, 1999, 1994; Yılmaz and Şengör, 1985; Yılmaz et al., 1997). However, new geological and radiometric age data have shown that this area consists of Middle Jurassic and Early Cretaceous subduction–accretionary complexes, which are collectively named the Central Pontide Supercomplex (CPS, Fig. 2; Marroni et al., 2014; Okay et al., 2013, 2006a). Within the CPS, Cretaceous *HP/LT* metamorphic rocks comprise an accretionary wedge consisting both of continental and oceanic crustal rocks. The continental accretionary rocks consist of a low-grade metaflysch sequence. Clastic zircon data from the metaclastic rocks exposed north of Araç town suggest that they represent metamorphosed equivalents of the Lower Cretaceous turbidites (Fig. 2; Okay et al., 2013). $^{40}Ar/^{39}Ar$ dating on phengites from this Martin Complex constrains the low-grade metamorphism as 112–106 Ma. Albian eclogites and a large ultramafic body are exposed at the northern part of the CPS, known as the Domuzdağ Complex (Fig. 2; Altherr et al., 2004; Okay et al., 2006a). The CPS is structurally underlain by a low-

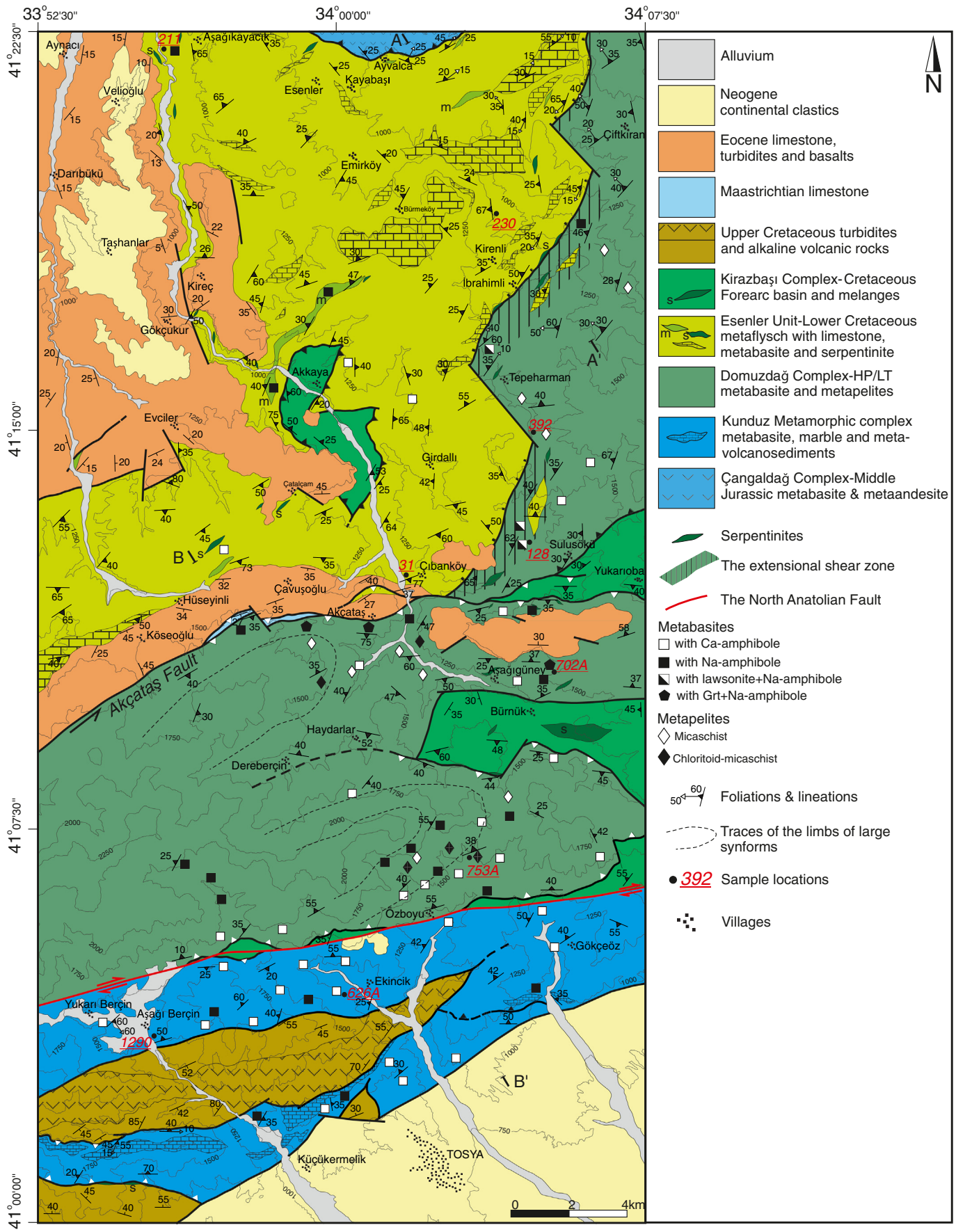

Fig. 3. Geological map of the region between Kastamonu and Tosya in the Central Pontides. See Fig. 2 for location.

grade metavolcanic unit, known as Kösdağ Formation exposed along the İAES as a tectonic slice (Rice et al., 2006; Tüysüz, 1990). It represents a Late Cretaceous (94 ± 2 Ma) juvenile intra-oceanic arc possibly associated with regional supra-subduction ophiolite obduction (Aygül et al., 2015a). $^{40}Ar/^{39}Ar$ dating on metamorphic muscovite constrains the regional metamorphism of the arc sequence to 70 Ma.

During this study we mapped a north–south transect across the CPS with the aim of characterizing continental and oceanic sequences and their contacts, determining age and grade of *HP/LT* metamorphism. Three major metamorphic units are distinguished (Figs. 3, 4): 1. In the northwest, a thick metasedimentary sequence, the Esenler Unit, shows incipient blueschist facies metamorphism. 2. The Esenler Unit is underlain by a tectonically thickened metamorphic sequence dominated by metabasic rocks. This Domuzdağ Complex has undergone a high-grade blueschist facies metamorphism, and 3. In the south, another metabasite–marble dominated unit with a low-grade blueschist facies metamorphism, the Middle Jurassic Kunduz Metamorphic Complex.

3. Subduction–accretionary wedge of the Central Pontides

3.1. Accreted distal turbidites: the Esenler Unit

The Esenler Unit is a metamorphosed flysch sequence composed predominantly of slate/phyllite and intercalated metasandstone (Fig. 5a) with lesser amounts of marble, metabasites and serpentinites. Metasandstones are mostly of greywacke type and occur as sheared pods within the slates. Recrystallized limestone blocks, up to 200 m across, in the metaflysch are interpreted as olistoliths. Barkurt et al. (1990) describe Lower Cretaceous fossils from these limestones. Most of the metabasites show incipient blueschist facies mineral assemblages and consist of sodic- and calcic-amphibole, sodic-pyroxene, epidote, chlorite, albite and titanite with augite relicts. Sheared serpentinite slices are found along shear zones. Temperature estimates based on Raman spectroscopy on carbonaceous material of the metapelitic rocks indicate that most of the Esenler Unit has undergone metamorphism at temperatures of ~330 °C but it also includes phyllite slices metamorphosed at higher temperatures of 370–385 °C (Aygül et al., 2015b).

North of the study area, the Esenler Unit is overthrust by low-grade metavolcanic rocks, which possibly form part of the Çangaldağ Complex (Figs. 3, 4a), a Middle Jurassic volcanic arc (Okay et al., 2006a, 2014; Ustaömer and Robertson, 1999). To the south, the Esenler Unit is separated from the Domuzdağ Complex by a detachment fault, partly overprinted by a post-Eocene east–west strike slip fault (Figs. 3, 4).

In terms of lithology, grade and age of metamorphism the Esenler Unit resembles metamorphosed Lower Cretaceous turbidites of the Martin Complex (Fig. 2). However, while the metabasites of Esenler Unit show incipient blueschist facies mineral assemblages, in the Martin Complex, they are of greenschist facies. We infer that the Esenler Unit represents distal segments of Lower Cretaceous turbidites deposited on the Laurasian active continental margin that were subsequently accreted.

3.2. Underplated oceanic metabasalts and metasediments: the Domuzdağ Complex

The Domuzdağ Complex is a blueschist to eclogite facies *HP/LT* metamorphic unit dominated by oceanic crustal lithologies indicating that it formed along an active margin and represents a subduction–accretionary complex (Altherr et al., 2004; Okay et al., 2006a; Tüysüz, 1990; Ustaömer and Robertson, 1999, 1994). In the area studied, the Domuzdağ Complex mainly consists of dark gray micaschist (about 40% of the sequence), metabasite (40%) and serpentinite (5%) with minor amounts of marble, metachert, and metagabbro (Fig. 5b, c). The mineral paragenesis in the micaschists is quartz + phengite + paragonite + chlorite + albite + rutile ± chloritoid ± garnet ± sodic amphibole. The metabasites are mostly well-foliated epidote-blueschists locally with garnet. The common mineral assemblage in the blueschists is sodic amphibole + epidote + chlorite + titanite + albite ± garnet. Eclogite facies mineral paragenesis was not found in the area studied. Retrogression to albite–chlorite fels is common with relicts of aligned sodic-amphibole. In terms of geochemistry, metabasites of the Domuzdağ Complex predominantly exhibit MORB and within-plate basalt characteristics (Ustaömer and Robertson, 1999).

3.2.1. The detachment fault

The detachment fault is an extensional shear zone of ca. 600 m in thickness that forms the main boundary between continental and oceanic accretionary units (Fig. 4a). It is characterized by mixing of blocks from the hanging- and foot-wall within a highly sheared brittle cataclasite. Marble, serpentinite, metabasite, and micaschist blocks are found along the shear zone (Fig. 6a). Metabasites consist of fresh lawsonite-blueschist and retrogressed albite–chlorite fels which were derived from the underlying Domuzdağ Complex. Lawsonite-blueschists predominantly consist of lawsonite and sodic-amphibole with additional sodic-pyroxene, chlorite, phengite, epidote, albite and titanite. Absence of lawsonite relicts in the albite–chlorite fels suggests that mixing of distinct metabasites occurred late during exhumation. NW dipping stretching lineations are observed within or around the shear zone, especially in the footwall micaschists which are characterized by absence of any peak metamorphic assemblages and the presence of syn-kinematic albite porphyroblasts. Blocks within the fault zone consistently indicate top to NW sense of shear (Fig. 6b). The detachment fault was responsible for the final exhumation of deeply buried metabasites and micaschists of the Domuzdağ Complex to shallow levels.

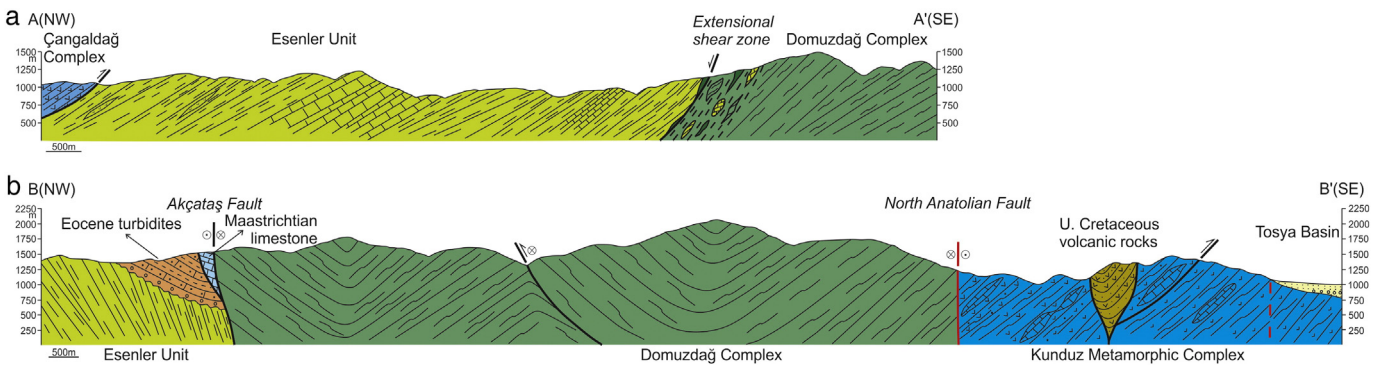

Fig. 4. Geological cross sections. See Fig. 3 for their locations. a) A–A′ section shows the initial structural relations between the Çangaldağ Complex, the Esenler Unit and the Domuzdağ Complex. b) B–B′ section shows the post-metamorphic faulting and folding between the Esenler Unit, Domuzdağ Complex and the Kunduz Metamorphic Complex.

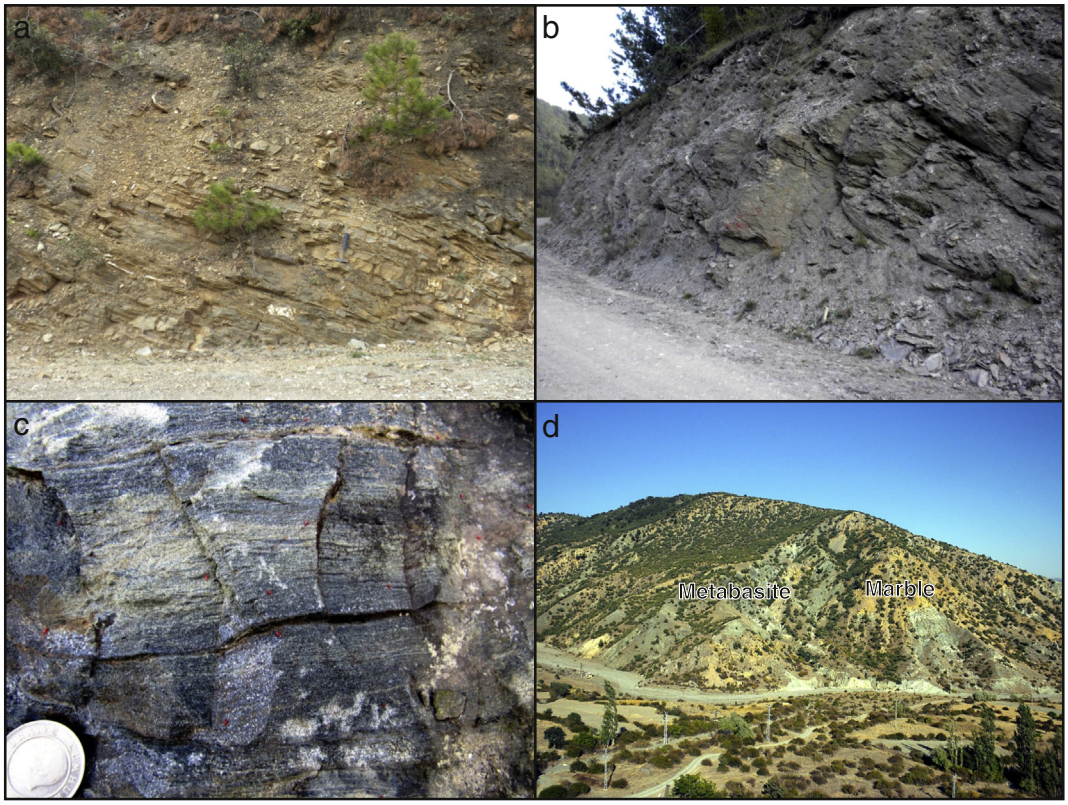

Fig. 5. Field photos of the units in the area studied. a) Slate and metasandstone intercalation of the Esenler Unit. b) Dark gray, carbonaceous micaschist of the Domuzdağ Complex. c) Well-foliated epidote-blueschist, Domuzdağ Complex. d) Metabasite and marble alternation of the Kunduz Metamorphic Complex.

3.3. Middle Jurassic accretionary complex: the Kunduz Metamorphic Complex

To the south, the Domuzdağ Complex is in contact with a metabasite–marble dominated unit along the North Anatolian Fault (Figs. 3, 4b). It consists of metabasites, volcanogenic metasandstones and metatuffs intercalated with pale marble horizons with minor metachert (Fig. 5d). The common mineral paragenesis in the metabasites is calcic-amphibole, epidote, chlorite, albite and titanite locally with sodic-amphibole. Metamorphism is dated here as Middle Jurassic with Albian overprint (see geochronology below). It forms the western extension of the so called Kunduz Metamorphics (Tüysüz, 1990).

Leucite-bearing alkaline volcanic rocks and volcanoclastic turbidites are widely exposed in the southern part of the accretionary prism. The volcanic sequence is reported to be of Campanian–Maastrichtian age (Rice et al., 2006). This is supported by recent $^{40}Ar/^{39}Ar$ age data on

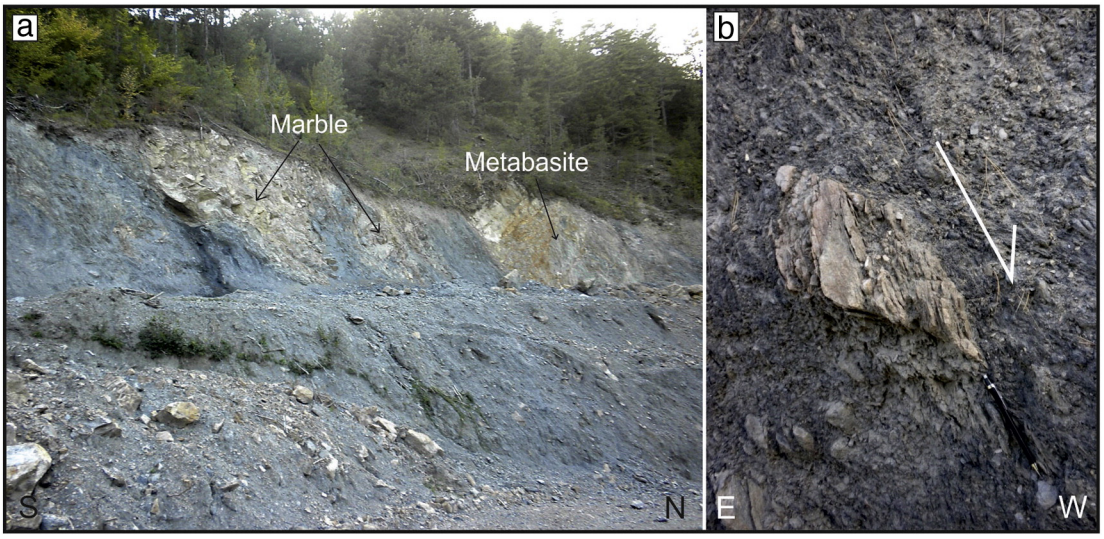

Fig. 6. Field photos of the extensional shear zone. a) General view of the shear zone with blocks of (from S to N) marble and a retrogressed metabasite within a gray cataclasite. b) A micaschist block within the cataclasite with NW sense of shear (pencil // lineation).

the alkaline volcanic rocks of 73.6 ± 0.18 and 76.78 ± 0.19 Ma (Genç et al., 2014). The volcanoclastic rocks were probably deposited on the Kunduz Metamorphic Complex, however, they now form a steeply dipping tectonic slice within the complex (Figs. 3, 4b). Geochemical data from the alkaline volcanic rocks show within-plate setting (Rice et al., 2006) and subduction-influenced volcanism (Genç et al., 2014, Gülmez et al., 2014). It is interpreted as a sedimentary-volcanic fill unit in a back-arc setting (Rice et al., 2006).

3.4. Cretaceous forearc basin and mélange: the Kirazbaşı Complex

The Central Pontide Supercomplex is overlain by an Upper Cretaceous volcano-sedimentary sequence. Most of the contacts of the volcano-sedimentary unit, called the Kirazbaşı Complex, with the metamorphic rocks are faulted. However, at few localities a stratigraphic contact is preserved (Okay et al., 2006a). In these localities the Kirazbaşı Complex starts with Turonian pelagic limestones, which pass up into siliciclastic turbidites overlain by mass flows and ophiolitic mélange, consisting of basalt, radiolarian chert, serpentinite, pelagic shale and limestone. Tüysüz and Tekin (2007) describe Cretaceous (Barremian to Cenomanian) radiolaria from the chert blocks. In the area studied, there are two main exposures of this unit. Around Akkaya village, reddish hemipelagic siltstone–shale alternations are overlain by a mélange-like slightly sheared greywacke and shales with pillow basalt and chert blocks. Around Bürnük, a clastic sedimentary sequence consisting of sandstone and siltstone is overlain by a mélange consisting of serpentinite, radiolarian chert, basalt, diabase and gray limestone blocks. The Kirazbaşı Complex is interpreted as a forearc basin developed in front of southward verging thrust slices in the accretionary prism.

4. Petrography and mineral chemistry

In order to determine the P–T conditions of the metamorphism, a metabasite from the Esenler Unit, a garnet-blueschist from the Domuzdağ Complex and a lawsonite-blueschist, exposed along the extensional shear zone, were analyzed by electron microprobe. Microprobe analyses were performed by a JEOL JXA8200 electron microprobe in the University of Potsdam using natural standards. Measurement conditions were 15 keV acceleration potential, 10 nA beam current and a beam diameter of 2–5 μm for counting times of 20 s. Representative mineral compositions are given in Table 1. Sample localities are shown in Fig. 3.

4.1. Metabasite within the Esenler Unit

Sample 211B is an unfoliated metabasite with augite relicts (Fig. 7a). The metamorphic mineral assemblage in the sample is sodic- and calcic-amphibole, sodic-pyroxene, epidote, chlorite, albite and titanite. Sodic-amphibole forms randomly distributed prismatic crystals and is of crossite composition (Fig. 8). Crossite is rimmed by actinolite. Sodic-pyroxene with a compositional range of $Aeg_{29-40}Jd_{6-13}Di_{53-58}$ overgrows and replaces magmatic augite. The Mg/(Mg + Fe) ratio of chlorites ranges between 0.57 and 0.47. Texturally, there are two types of epidote. The first one forms large grains with iron-rich cores (Fe^{3+}/(Fe^{3+} + Al) = 0.36). The Fe# ratio decreases rimward to 0.23–0.24. The second type forms small grains with pistacite-poor cores (Fe^{3+}/(Fe^{3+} + Al) = 0.14–0.17) and Fe–rich rims (Fe^{3+}/(Fe^{3+} + Al) = 0.29–0.31). The stable Ti–bearing phase is titanite. Plagioclase is almost pure albite (An = 0–1%).

4.2. Lawsonite-blueschist block within the extensional the shear zone

The lawsonite-blueschist (sample 128) consists of sodic-amphibole, lawsonite, sodic-pyroxene, chlorite, phengite, epidote, albite and titanite (Fig. 7b). Sodic-amphibole has crossitic cores rimmed by glaucophane (Fig. 8). Glaucophane also forms single grains and is found as inclusion in lawsonite. Sodic-amphibole is partly replaced by albite and chlorite. Lawsonite is partly decomposed to epidote and albite along its rims. Sodic-pyroxene shows two compositional ranges: $Jd_{4-18}Aeg_{31-23}Di_{65-59}$ and $Jd_{25-36}Aeg_{32-28}Di_{43-37}$. Si content of phengites ranges between 3.41 and 3.54 silicon per formula unit (p.f.u.). Epidote has pistacite-poor cores (Fe^{3+}#: 0.02–0.09) and Fe^{3+} rich rims (Fe^{3+}#: 0. 23–0.33). Chlorite (Mg/(Mg + Fe) = 0.53–0.54) replaces the Na-clinopyroxene. Plagioclase is albite (An = 0–5%) and Ti-bearing phase is titanite.

4.3. Garnet-blueschist from the Domuzdağ Complex

The garnet-blueschist (sample 702 A) consists of garnet, sodic- and calcic-amphibole, epidote, chlorite, albite, phengite, titanite and magmatic augite relicts (Fig. 9a). Garnets grow over the foliation defined by glaucophane and epidote. They are 0.2 to 0.4 mm across and comprise glaucophane, epidote, and titanite inclusions aligned parallel to the main foliation. Generation of pressure shadows defined by glaucophane, epidote and phengite suggests a syn-kinematic origin (Fig. 9a). Compositional range of the garnet is $Alm_{44-56}Py_{2-4}Grs_{39-38}Sps_{15-2}$. From core to rim, almandine increases at the expense of spessartine but the sum of these components remains stable with little change in the grossular and pyrope contents. This can also be seen in element maps showing a typical garnet growth zoning evidenced by progressive exchange of Fe and Mn (Fig. 9b).

Sodic-amphibole is mostly ferroglaucophane (Fig. 8) and replaces augites along their rims or forms aligned prismatic crystals that define the foliation. Sodic-amphibole is rimmed and partly replaced by calcic-amphibole and chlorite. Epidote has pistacite-poor core (Fe^{3+}# = 0.06–0.12) and pistacite-rich rim (Fe^{3+}# = 0.18–0.22). Si contents of phengite range between 3.41 and 3.53 c.p.f.u. Within the garnet pressure shadows, Si content of phengite decreases rimward (3.50–3.44 c.p.f.u). Mg/(Mg + Fe) of chlorite ranges between 0.48 and 0.56. The stable Ti-bearing phase is titanite. Plagioclase is albite (An = 1–6%).

5. Pressure–temperature estimates of the metamorphism

To constrain the PT conditions of the lawsonite- and garnet-blueschists, we produced pseudosections by Theriak-Domino software calculating equilibrium mineral assemblages by the Gibbs free energy minimization method (de Capitani and Brown, 1987; de Capitani and Petrakakis, 2010). Bulk rock chemistry was obtained by XRF analysis in GeoForschungsZentrum (GFZ), Potsdam (Table 2).

5.1. Lawsonite-blueschist (sample 128)

In the modeled PT space sudden increase of jadeite and decrease of diopside contents of sodic-pyroxene ($Jd_{4-18}Aeg_{31-23}Di_{65-59}$ and $Jd_{25-36}Aeg_{32-28}Di_{43-37}$) overlaps with the first appearance of the lawsonite (Fig. 10a). The peak mineral assemblages of lawsonite + glaucophane + sodic-pyroxene + phengite for the sample 128 cover a large P–T area. According to X_{Jd} of omphacite and Si contents of phengite, we constrained the metamorphic conditions to 12–16 kbar pressure and 370–440 °C temperature (Fig. 10a).

5.2. Garnet-blueschist (sample 702A)

For the sample 702A, garnet grows at the expense of epidote. In the shaded area of Fig. 10b, with increasing pressure, X_{Grs} increases and X_{Alm} decreases. In sample 702A, grossular component is stable around 40%. This suggests that garnet growth occurred along a path parallel to the X_{Grs} isopleths (Fig. 10b). In the shaded area, Si isopleths of phengite are orthogonal to the X_{Grs} and X_{Alm} isopleths and X_{Si} decreases along the inferred path. This is in accordance with measured phengite

Table 1
Representative mineral compositions.

	211B			Core	Rim		128							Core
	Amph	Amph	Na-cpx	Ep	Ep	Chl	Amph	Amph	Lws	Lws	Na-cpx	Na-cpx	Ms	Ep
	252	249	321	240	241	267	178	171	155	170	140	147	144	158
SiO_2	53.93	52.63	52.02	38.13	37.28	29.92	56.57	56.97	38.65	38.50	53.88	55.43	51.74	39.33
TiO_2	0.05	0.04	0.08	0.13	0.04	0.04	0.15	0.08	0.40	0.04	0.00	0.08	0.04	0.06
Al_2O_3	4.98	1.37	2.55	28.55	22.69	16.13	5.96	9.65	31.46	31.89	2.80	9.17	23.60	30.58
Cr_2O_3	0.01	0.00	0.02	0.00	0.01	0.00	0.00	0.02	0.02	0.02	0.00	0.00	0.00	0.00
FeO	23.43	17.87	15.99	6.74	13.91	23.00	17.77	15.46	0.59	0.83	13.43	12.08	4.03	4.39
MnO	0.17	0.26	0.22	0.15	0.13	0.29	0.29	0.12	0.06	0.00	0.61	0.27	0.05	0.20
MgO	6.52	12.82	7.25	0.02	0.00	17.24	9.39	8.23	0.03	0.01	8.44	5.13	4.08	0.00
CaO	0.75	10.77	13.11	23.06	22.40	0.23	1.36	0.50	16.85	16.95	15.12	9.41	0.03	24.05
Na_2O	6.45	1.00	5.33	0.02	0.00	0.03	6.81	7.49	0.01	0.01	5.50	9.03	0.08	0.01
K_2O	0.09	0.10	0.04	0.01	0.01	0.48	0.01	0.02	0.01	0.01	0.01	0.01	11.45	0.05
Total	96.37	96.86	96.63	96.79	96.47	87.35	98.32	98.54	88.07	88.25	99.77	100.60	95.11	98.66
Si	7.884	7.737	2.002	2.974	2.981	3.122	7.923	7.904	2.031	2.022	1.989	1.982	3.509	2.992
Ti	0.006	0.004	0.002	0.008	0.002	0.003	0.016	0.008	0.016	0.002	0.000	0.002	0.002	0.004
Al	0.858	0.238	0.116	2.624	2.139	1.984	0.984	1.577	1.949	1.974	0.122	0.386	1.887	2.742
Cr	0.001	0.000	0.274	0.000	0.000	0.000	0.000	0.002	0.001	0.001	0.000	0.000	0.000	0.000
Fe^{3+}	1.172	0.547	0.001	0.439	0.930	0.000	0.880	0.428	0.000	0.000	0.294	0.271	0.000	0.279
Fe^{2+}	1.692	1.650	0.240	0.000	0.000	2.007	1.201	1.365	0.026	0.036	0.120	0.090	0.228	0.000
Mn	0.021	0.033	0.007	0.010	0.009	0.025	0.035	0.014	0.002	0.000	0.019	0.008	0.003	0.013
Mg	1.421	2.809	0.416	0.002	0.000	2.681	1.961	1.701	0.003	0.000	0.464	0.274	0.412	0.000
Ca	0.117	1.697	0.541	1.927	1.919	0.025	0.204	0.075	0.949	0.954	0.598	0.360	0.002	1.960
Na	1.828	0.285	0.398	0.002	0.000	0.006	1.849	2.015	0.001	0.001	0.393	0.626	0.011	0.002
K	0.016	0.019	0.002	0.001	0.001	0.064	0.002	0.004	0.001	0.000	0.000	0.000	0.991	0.005
Total	15.016	15.019	4.000	7.988	7.982	9.918	15.055	15.094	4.979	4.990	4.000	4.000	7.046	7.997

Mineral fornmula calculations are based on 23 oxygen for Amph, 4 cations for Cpx; 12.5 oxygen for Ep; 14 oxygen for Chl; 8 oxygen for Lws and Ab; 11 oxygen for Ms; 12 oxygen for Grt. Amphibole formula is calculated by an existed exel spreadsheet based on maximum ferric iron correction after Schumacher (1997); for sample 128 and 702A, normalized to 13eCNK and for sample 211B to 15eK.

composition in the garnet pressure shadow. Modeled clinopyroxene composition forms hedenbergite and diopside solid solution. Jadeite component appear in the high pressure part of the PT area after consumption of epidote (X_{Jd}: ~3%). However, no growth of metamorphic clinopyroxene is detected in sample 702A but relicts of augites. Metamorphic conditions are constrained as 17 ± 1 Kbar and 500 ± 40 °C.

5.3. Metabasite of the Esenler Unit (sample 211B)

PT conditions of the sample 211B are weakly constrained by single reactions (Fig. 11) calculated by TERMOCALC (3.33) software (Powell and Holland, 1988) using the thermodynamic data set of Holland and Powell (1998). Activities of the reactions were calculated from the mineral chemistries by the AX program (https://www.esc.cam.ac.uk/research/research-groups/holland/ax). A petrogenetic grid for the low-grade metabasite in NCMASH system (Schiffman and Day, 1999) and stabilities of the sodic-, sodic–calcic and calcic amphibole (Otsuki and Banno, 1990) are also added in Fig. 11. The presence of albite gives the upper limit of the pressure. A lower limit of pressure is constrained by reaction (1);

$$Daph_{0.012} + Ab + Fact_{0.0045} = Fgl_{0.0132} + Cz_{0.53} + Qtz + H_2O. \quad (1)$$

A possible lower limit of the temperature is constrained by the absence of lawsonite by the following reactions;

$$Fgl_{0.0132} + Lws = Ab + Qtz + Daph_{0.012} + Cz_{0.53} + H_2O \quad (2)$$

$$Gl_{0.0061} + Law = Cz_{0.53} + Ab + Qtz + Ames_{0.021} + H_2O. \quad (3)$$

Metamorphic conditions were constrained as 400 ± 70 °C temperatures and 7–12 kbar pressures.

6. Structural analysis of the accretionary wedge

In the Central Pontides, general regional structures of accretionary wedge trend in SW–NE direction which has been subjected up to 40° Late Cretaceous–Paleocene counter-clockwise rotation revealed by paleomagnetic studies (Meijers et al., 2010). In the study area, this trend is represented by the detachment fault separating the Esenler Unit from the underlying Domuzdağ Complex. Similar contact relations are also observed in the NW of the study area where the Domuzdağ Complex is overlain by the Çangaldağ Complex (Okay et al., 2006a). Orientation of foliation planes of the Esenler Unit varies depending on their proximity to different contacts (Fig. 12a). In the north of the study area, the Esenler Unit is overthrust by the metavolcanic rocks of the Çangaldağ Complex. Around the thrust, strong stretching lineation developed in the metaflysch and the metavolcanic rocks trending SW–NE and slightly plunging to NE (Fig. 12b). Lineations with similar trends are common throughout the metaflysch suggesting a general transport in this direction. These remarkable SW–NE trending lineations are also reported farther east from the Çangaldağ Complex overlying the Domuzdağ Complex (Okay et al., 2006a). They are oblique to the general structural trend of the Central Pontides and may depict the obliquity of the subduction itself.

To the south of the detachment fault, foliation planes of the Domuzdağ Complex strike SW–NE parallel to the detachment (Fig. 12c). The footwall micaschists predominantly exhibit NW plunging stretching lineation orthogonal to the foliation (Fig. 12d). Similar lineations are also observed in the blocks and fault gouge of the extensional shear zone. This suggests that they developed by pervasive shearing during exhumation.

An east–west striking post-Eocene fault, the Akçataş Fault (Figs. 3, 4b), overprints the detachment fault and separates the Domuzdağ Complex into two sectors. Along the Akçataş fault, the Domuzdağ Complex thrusted over the Esenler Unit which also shows an inverted metamorphic grade revealed by the temperatures obtained from Raman spectra of carbonaceous material (Aygül et al., 2015b). South of the Akçataş fault, foliation planes of the Domuzdağ Complex define large synforms (Figs. 12e, 4b)

Rim			702A		Core	Rim	Core	Rim	Core	Rim				
Ep	Chl	Ab	Amph	Amph	Grt	Grt	Ep	Ep	Ms	Ms	Chl	Cpx	Cpx	Ab
156	153	187	20	1	35	34	31	32	27	28	29	52	89	57
37.92	29.08	69.21	56.34	55.96	37.14	37.27	38.96	38.10	53.47	50.94	26.69	50.38	50.54	68.55
0.06	0.03	0.00	0.07	0.03	0.19	0.15	0.08	0.17	0.11	0.12	0.02	1.18	1.00	0.00
24.11	19.67	19.46	10.29	12.05	20.87	21.31	31.11	25.96	25.70	25.11	19.43	3.62	4.10	19.48
0.01	0.01	0.00	0.02	0.01	0.00	0.00	0.03	0.00	0.00	0.00	0.03	0.06	0.38	0.00
12.25	23.51	0.15	15.58	15.92	22.12	25.43	3.46	9.63	4.05	4.22	27.08	9.28	8.74	0.17
0.41	0.36	0.02	0.11	0.12	5.06	1.04	0.02	0.03	0.04	0.04	0.14	0.23	0.25	0.01
0.02	15.13	0.01	7.55	6.28	0.45	0.57	0.00	0.00	3.85	3.62	14.16	15.13	16.56	0.00
22.70	0.12	0.14	1.40	0.52	14.11	13.97	24.20	23.35	0.04	0.01	0.03	19.84	18.20	0.13
0.00	0.16	11.86	6.72	7.66	0.02	0.04	0.04	0.02	0.11	0.14	0.04	0.38	0.40	11.83
0.00	0.17	0.03	0.02	0.06	0.01	0.01	0.01	0.01	9.73	11.30	0.08	0.00	0.00	0.02
97.48	88.24	100.89	98.10	98.60	99.96	99.79	97.90	97.26	97.11	95.51	87.69	100.09	100.16	100.19
2.988	2.995	2.999	7.883	7.825	2.970	2.973	2.981	2.986	3.500	3.442	2.836	1.864	1.856	2.992
0.004	0.002	0.000	0.007	0.003	0.011	0.009	0.005	0.010	0.005	0.006	0.002	0.033	0.028	0.000
2.239	2.389	0.993	1.697	1.986	1.967	2.003	2.805	2.398	1.983	2.000	2.432	0.158	0.177	1.002
0.000	0.001	0.000	0.002	0.001	0.000	0.000	0.002	0.000	0.000	0.000	0.002	0.002	0.011	0.000
0.807	0.000	0.000	0.274	0.115	0.000	0.000	0.221	0.631	0.000	0.000	0.000	0.073	0.073	0.000
0.000	2.026	0.005	1.549	1.747	1.479	1.696	0.000	0.000	0.222	0.239	2.406	0.214	0.196	0.006
0.027	0.031	0.001	0.013	0.014	0.343	0.070	0.001	0.002	0.002	0.002	0.012	0.007	0.008	0.000
0.003	2.323	0.001	1.575	1.309	0.053	0.068	0.000	0.000	0.376	0.365	2.243	0.835	0.907	0.000
1.916	0.013	0.007	0.210	0.078	1.209	1.193	1.983	1.961	0.003	0.001	0.004	0.787	0.716	0.006
0.000	0.033	0.996	1.824	2.077	0.002	0.006	0.006	0.004	0.013	0.018	0.007	0.027	0.029	1.001
0.000	0.023	0.002	0.004	0.010	0.001	0.001	0.001	0.000	0.813	0.974	0.011	0.000	0.000	0.001
7.985	9.836	5.004	15.038	15.165	8.037	8.020	8.005	7.992	6.917	7.048	9.954	4.000	4.000	5.008

bound by faults parallel to the Akçataş Fault. Such a fold pattern is also observed within the Kunduz Metamorphic Complex (Fig. 12f) and also in the Campanian alkaline volcanic and volcano-clastic rocks. This post-metamorphic deformation is likely to be associated with the accretion of the Kösdağ Arc at ca. 70 Ma (Aygül et al., 2015a).

7. $^{40}Ar/^{39}Ar$ geochronology

In order to constrain the age of regional metamorphism, we dated phengite separates from the Esenler Unit, the Domuzdağ and the Kunduz metamorphic complexes by $^{40}Ar/^{39}Ar$ method (for the sample location see Fig. 3). Dating was conducted at the $^{40}Ar/^{39}Ar$ geochronology laboratory of University of Potsdam by stepwise heating with CO_2 laser. The dating system and the procedures are given in recent literature including, Aygül et al. (2015a); Halama et al. (2014) or Wilke et al. (2010). Details of the procedures of the analysis and calculation are given as an electronic supplementary file (Appendix A1). All the results are shown by the age spectra in Fig. 13. The $^{40}Ar/^{39}Ar$ data are provided in Appendix A2 (Table A2) and microphotographs of the dated samples are presented in Appendix A3.

7.1. Cretaceous HP/LT metamorphism

Samples 31 and 230 are phyllites from the Esenler Unit. They show similar mineralogical composition and texture and consist of white mica, quartz, chlorite, and albite. Fine grained phengite and chlorite define the foliation. Sample 392 is a micaschist from the Domuzdağ Complex exposed south of the detachment fault. It consists of phengite, paragonite, chlorite, quartz, rutile and syn-kinematic albite porphyroblasts with rotational inclusion fabrics. Foliation is

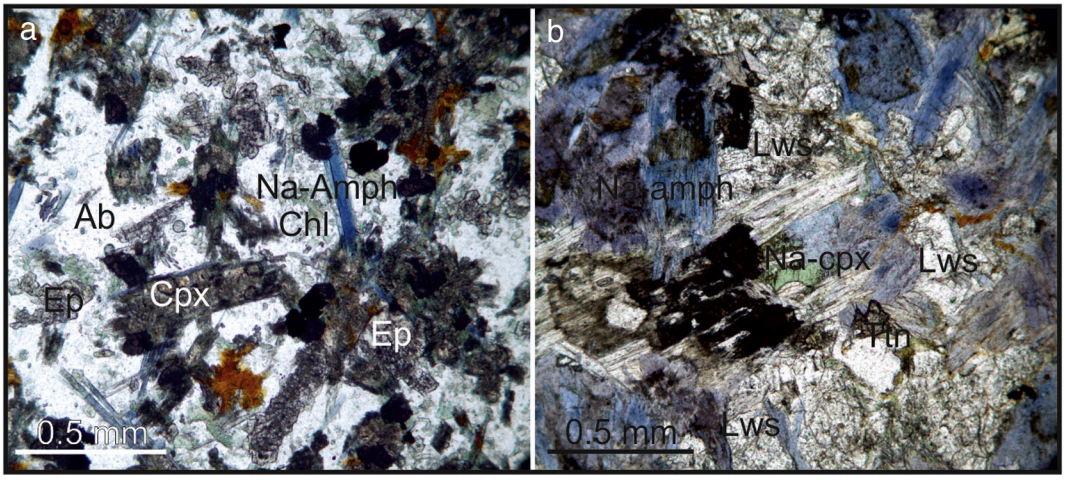

Fig. 7. Plane-polarized photomicrographs of (a) an unfoliated metabasite from the Esenler Unit (sample 211B) and (b) a lawsonite-blueschist exposed along the extensional shear zone (sample 128). Na-amph = sodic amphibole; Cpx = augite relicts; Ep = epidote; Chl = chlorite; Ab = albite; Lws = lawsonite; Na-cpx = sodic clinopyroxene; Ttn = titanite.

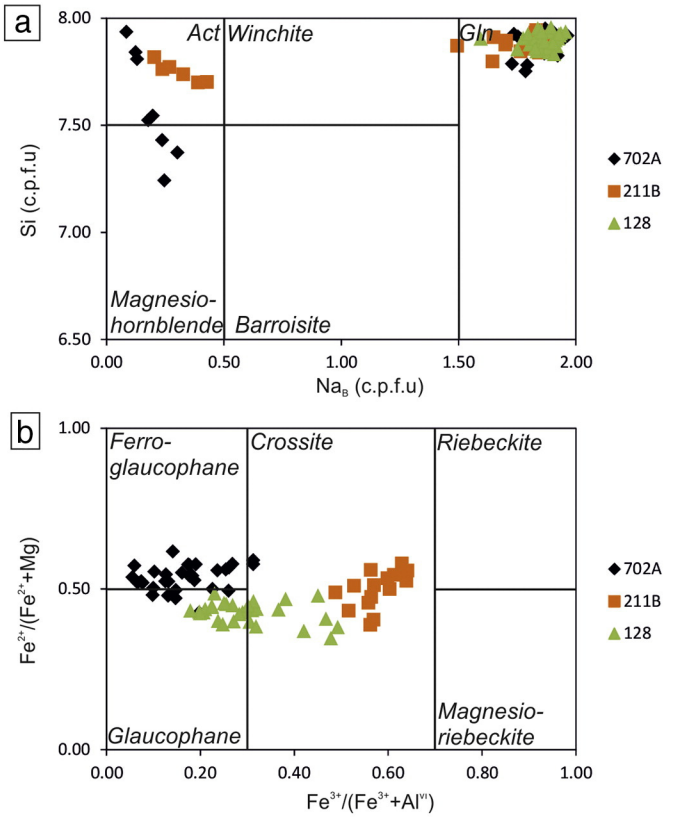

Fig. 8. Compositional ranges of the amphiboles of the measured metabasites. Sample 211B is the metabasite within the Esenler Unit; sample 128 is the lawsonite-blueschist exposed along the extensional shear zone and sample 702A is a garnet-blueschist from the Domuzdağ Complex.

Table 2
Bulk rock compositions and calculated element mol percentages used in the pseudo-section calculations.

	128	702A
Oxide (wt.%)		
SiO_2	50.21	46.39
TiO_2	1.56	2.01
Al_2O_3	14.91	14.25
Fe_2O_3	11.99	13.71
MnO	0.17	0.23
MgO	5.28	6.51
CaO	6.09	8.98
Na_2O	4.40	2.85
K_2O	0.66	0.57
P_2O_5	0.16	0.24
LOI	4.38	3.95
Total	99.80	99.70
Element (mol%)		
Si	22.228	22.284
Al	7.891	7.421
Ti		1.206
Fe	8.386	9.589
Mg	3.184	3.926
Ca	3.184	6.518
Na	3.264	2.114
K	0.548	0.473
H_2O	Saturated	Saturated

defined by phengite (3.33–3.48 Si c.p.f.u) and chlorite. Sample 753A is a chloritoid-micaschist consisting of chloritoid, phengite, chlorite, paragonite, quartz and rutile with pseudomorphs after glaucophane. Chloritoid forms porphyroblasts of radially growing crystals. Foliation, defined by phengite and chlorite, bends around the chloritoid porphyroblasts. Si content of phengite ranges between 3.23 and 3.47 c.p.f.u.

T-
he

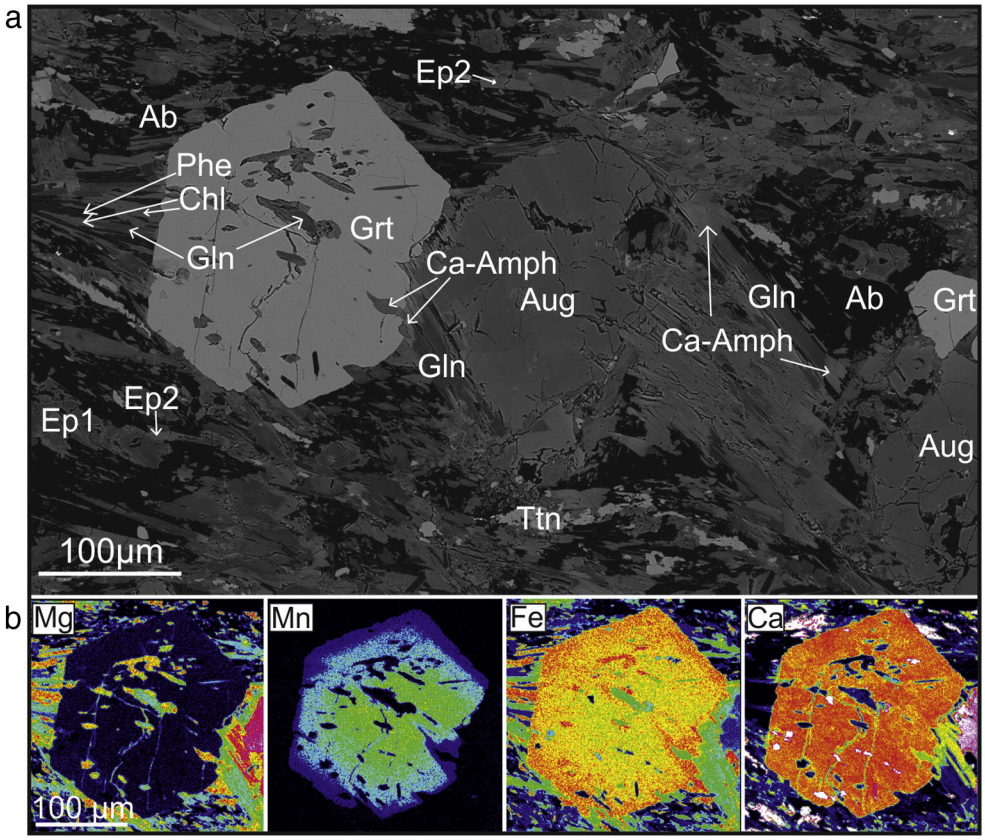

Fig. 9. a) BSE image of the garnet-blueschist (702A). Garnet exhibit pressure shadow consisting of Gln + Phe + Ep. Ca-amph, Chl and Ab are secondary and replace Na-amphiboles elsewhere. b) Element mapping of the garnet in Fig. 8a with typical growth zoning. Ca and Mg are almost stable. Mn decreases rimward while Fe increases.

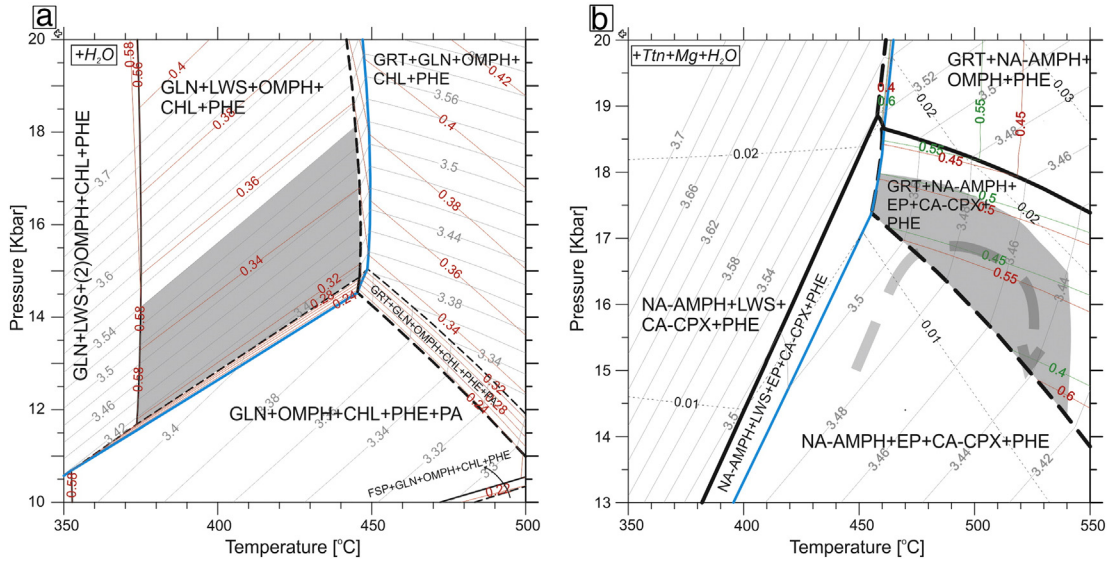

Fig. 10. Pseudosections produced by the Theriak-Domino software showing calculated equilibrium mineral assemblages for the metabasites. a) Modeled PT space for lawsonite-blueschist (sample 128). The peak mineral assemblages of Lws + Gln + Na-Cpx + Phe are labeled. Thick blue line limits the stability field of lawsonite, thick dashed line garnet and thin dashed line for the paragonite. Thick black line limits the stability of albite at the lower part of diagram. According to X_{Jd} (red) and Si isopleths (gray) of phengite metamorphic conditions constrained as 14 ± 2 kbar and 370–440 °C (shaded area). b) Modeled PT space for the garnet-blueschist (702A). Thick black line limits stability field of epidote and dashed line of garnet. Stability field of lawsonite is marked by thick blue line. Isopleths; gray, Si content of phengite; green and red, X_{Grs} and X_{Alm}, respectively; dashed isopleth, X_{Jd}. Metamorphic conditions constrained as 17 ± 1 kbar and 500 ± 40 °C (shaded area). (For interpretation of the references to color in this figure legend, the reader is referred to the online version of this chapter.)

$^{40}Ar/^{39}Ar$ phengite ages of the samples 31 and 230 are 101.5 ± 4.8 Ma and 99.9 ± 1.7 Ma, respectively, and agree within 1 sigma error limits (Fig. 13a, b) and indicate a late Early Cretaceous regional metamorphism for the distal turbidites. Sample 392 exhibits a plateau age of 100.6 ± 1.3 Ma (Fig. 13c). Sample 753A, however, gives a younger plateau age of 91.8 ± 1.8 Ma than three ages above (Fig. 13d). The age

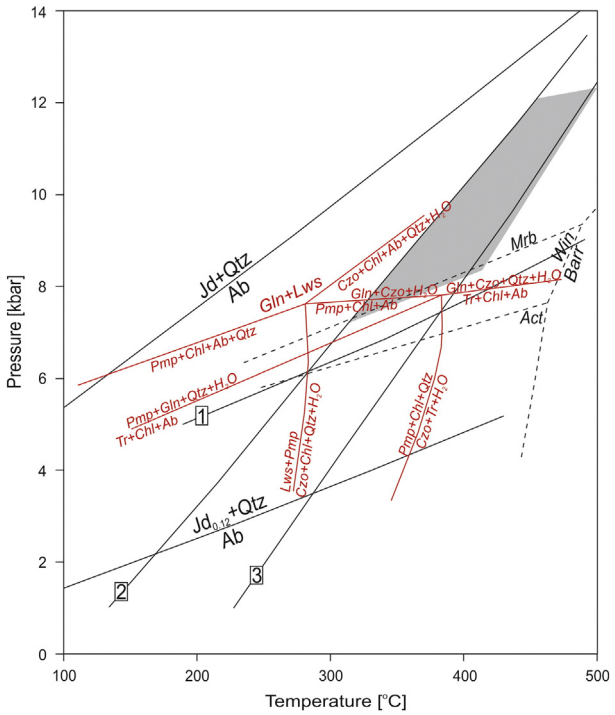

Fig. 11. *PT* estimates of the sample 211B (shaded area) by single reactions produced by THERMOCALC software. Stabilities of the amphiboles are from Otsuki and Banno (1990) and a petrogenetic grid in NCMASH system for low-grade metabasite is from Schiffman and Day (1999). Jd = jadeite; Qtz = quartz; Ab = albite; Mrb = magnesioriebeckite; Win = winchite; Barr = barroisite; Act = actinolite; Gln = glaucophane; Lws = lawsonite; Pmp = pumpellyite; Chl = chlorite; Czo = clinozoisite; Tr = tremolite.

results are in accordance with previously published data constraining the regional metamorphism in the Central Pontides as Albian (Okay et al., 2013, 2006a). The 91.8 ± 1.8 Ma age, the youngest $^{40}Ar/^{39}Ar$ age obtained in Central Pontides so far, indicates that subduction and accretion continued until Turonian with a possible southward younging of the H*P/LT* regional metamorphism.

Interpretation of the radiogenic ages depend on the isotopic closure concept accepting temperature as fundamental parameter together with grain size and cooling rate (Dodson, 1973). Additionally deformation and fluids have a significant effect on isotopic diffusion (Villa, 1998). Harrison et al. (2009) report a closure temperature of muscovite grain 100 μm across, cooling at 10 °C/Ma at 10 kbar as 425 °C. The relatively low temperatures of metamorphism (~380 °C for the Esenler Unit and 450–500 °C for the Domuzdağ Complex) indicate that the obtained ages represent crystallization. In sample 392, however, the obtained age should be an exhumation age related to recrystallization by extensional shearing. This is evidenced by i) its structural position close to the extensional shear zone with identical lineation development and ii) absence of any peak metamorphic assemblages but syn-kinematic albite porphyroblasts. The 91.8 ± 1.8 Ma age suggests that extensional shearing and exhumation of the footwall micaschist occurred during on-going subduction.

Early–Middle Eocene limestones lie unconformably over the metamorphic rocks of the CPS (Okay et al., 2013; Özcan et al., 2007). In the area studied, Helonocyclina and Orbitoides-bearing Maastrichtian limestones (Ercan Özcan, per. com.) exposed along the post-Eocene Akçataş strike-slip fault and Campanian alkaline volcanic rocks (Genç et al., 2014) provide an upper age limit for the regional metamorphism.

7.2. Middle Jurassic HP/LT metamorphism

Two samples from the Kunduz Metamorphic Complex yielded Middle Jurassic $^{40}Ar/^{39}Ar$ phengite ages. The first sample (626A) is a quartz-micaschist interlayered with light colored marble and metabasite. It consists of quartz, phengitic white mica, epidote, hematite and titanite. Phengites define a weakly developed foliation. Their Si contents range between 3.37 and 3.44 c.p.f.u. The second sample (1290) is a well-foliated metatuff consisting of quartz, phengite, albite, bluish-green amphibole,

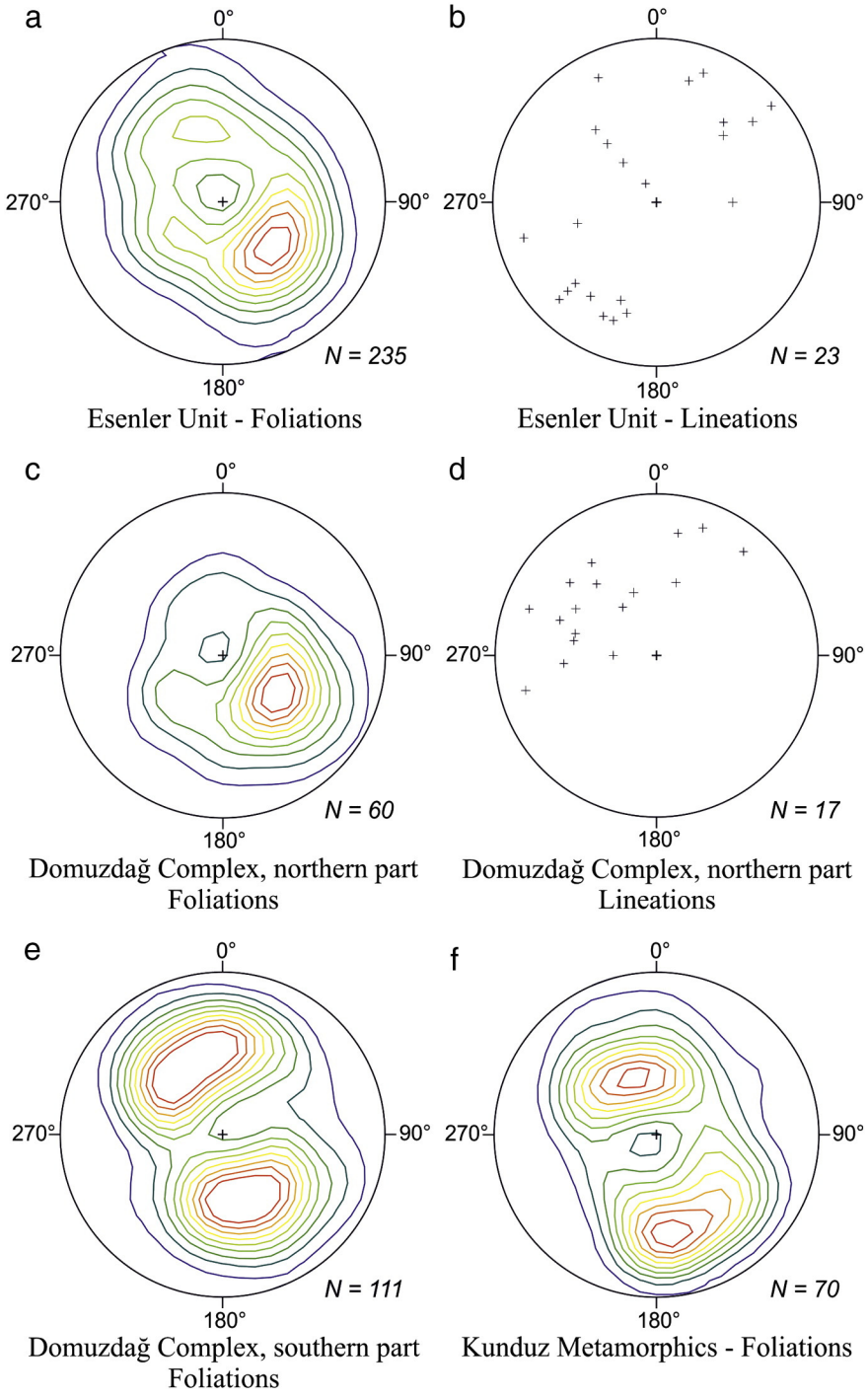

Fig. 12. Lower hemisphere, equal area projections of the foliations and the lineations. a) Foliation and b) lineation data from the Esenler Unit. c) Foliation and d) lineation measurements of the northern part of the Domuzdağ Complex. Lineations are mostly orthogonal to the NW dipping foliation planes and plunge to the NW related exhumation. e) Foliation data from the southern part of the Domuzdağ Complex and f) the Kunduz Metamorphic Complex.

chlorite and stilpnomelane with magmatic augite relicts. Amphibole replaces the augite. Phengite defines the foliation.

The $^{40}Ar/^{39}Ar$ phengite age of the sample 626A is constrained as 159.3 ± 1 Ma with a pronounced plateau (Fig. 13e). Sample 1290 exhibits, however, a disturbed plateau possibly associated with mixing of different generation of the phengites. Released radiogenic ^{40}Ar is concentrated in 151–161 Ma (Middle Jurassic) in the middle temperature steps and ca. 100 Ma (Albian) with a 101 ± 0.6 Ma in the last 5 steps making an apparent short "plateau" within the steps (Fig. 13f). Due to the fact that radiogenic ^{40}Ar was predominantly released in the third and fourth steps which also hold >50% of the cumulative released ^{39}Ar (Table A2), we infer a Middle Jurassic age for the sample which is possibly overprinted during the Albian orogeny.

8. Discussion

Middle Jurassic and Cretaceous *HP/LT* metamorphic rocks, collectively named as Central Pontide Supercomplex (CPS), crop out widely in the central part of the Pontides (Okay et al., 2013). In the Pontides, Middle Jurassic subduction–accretionary complexes (Çelik

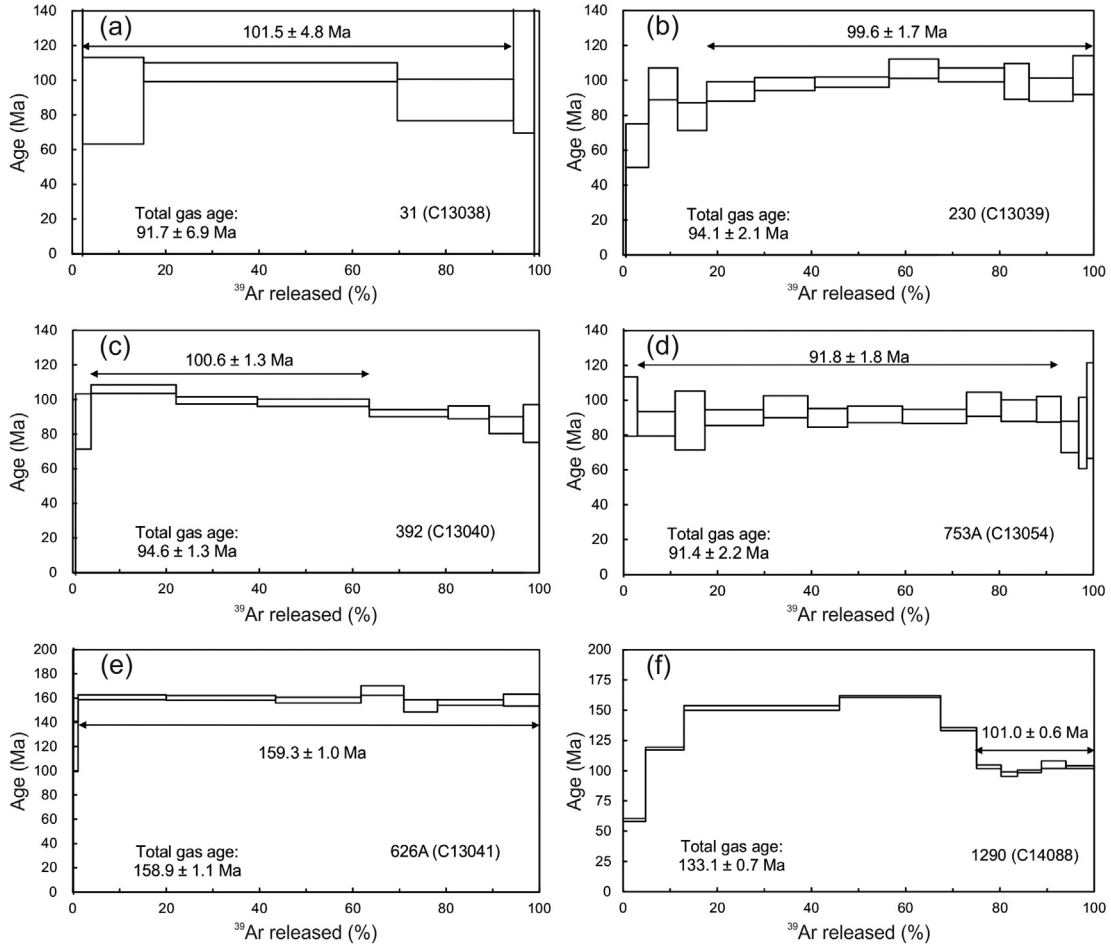

Fig. 13. $^{40}Ar/^{39}Ar$ age spectra of the analyzed phengites in this study. a and b: obtained from the accreted distal turbidites (the Esenler Unit). c and d: Micaschists from the Domuzdağ Complex. e and f: Obtained from the Kunduz Metamorphic Complex. The age values shown are the weighted mean of the selected steps as shown in each figure. Plateau ages are shown from (a) to (e).

et al., 2011; Marroni et al., 2014; Okay et al., 2013; Topuz et al., 2012) or arc sequences consisting of volcanic and intrusive rocks with *LP/HT* metamorphic rocks (Genç and Tüysüz, 2010; Göçmengil et al., 2013; Okay et al., 2014) are increasingly reported in the last several years. This suggests that Middle Jurassic represents a period of convergence in Tethyan realm. In the CPS, the Middle Jurassic accretionary complexes lie south of the Albian–Turonian ones, contrary to what is expected in an evolving accretionary-type orogen. The possible Albian metamorphic overprint in the Middle Jurassic metamorphic rocks suggests that tectonic emplacement occurred during Albian orogeny. Subduction obliquity can cause significant along strike tectonic transport by using zones of weakness (e.g. Beck, 1983; Fitch, 1972; Jarrard, 1986; McCaffrey, 1992). Emplacement of the Middle Jurassic metamorphic rocks is most probably related to oblique convergence of the Albian subduction.

The Cretaceous units within the CPS represent an Albian–Turonian accretionary wedge along the Laurasian active continental margin. The Albian–Turonian wedge is divided into a continental unit in the north and an oceanic one in the south. The continental accretionary units, the Martin Complex and the Esenler Unit, represent accreted distal parts of Lower Cretaceous turbidites suggesting significant amount of clastic sediment supply from a continental domain to the north (Fig. 2; Aygül et al., 2015b; Okay et al., 2013). This has a primary effect on frontal enlarging of the wedge by offscraping and shallow level underplating of continental detritus (Aygül et al., 2015b). The accreted distal turbidites are tectonically underlain by oceanic crust-derived *HP/LT* metabasite and micaschist along a detachment fault. In the area studied, the deep-seated metabasites are epidote-blueschist locally with garnet. Lawsonite-blueschist blocks within the extensional shear zone indicate a major break in the metamorphic grade. The tectonic position of the lawsonite-blueschists suggests that they formed during earlier stages of the accretion along the overriding plate boundary. Lawsonite stability is generally regarded as indicative for relatively cold thermal setting and fast exhumation (Tsujimori et al., 2006b; Whitney and Davis, 2006; Zack et al., 2004). There are many parameters that can affect the thermal structure of a subduction zone including age of the slab, convergence rate, geometry of subduction, and shear related heating (Peacock, 1996). It is reported by numerical modeling that temperatures at the upper part of a subduction zone along the plate contact are primarily determined by frictional heating (van den Beukel and Wortel, 1987). Accordingly, Peacock (1992) showed that occurrence of blueschist facies low temperatures rocks is associated with low shear stress and low shear heating along the subduction zone. We infer that during the initial stage of the Albian convergence, accretion was characterized by low shear stress generating a relatively cold thermal structure where the lawsonite-blueschists formed.

8.1. Tectonic thickening of the deep-seated Domuzdağ Complex

In the central Pontides, the deep-seated oceanic Domuzdağ Complex comprises a major proportion of the Albian–Turonian wedge and consists of a tectonically thickened eclogite to blueschist facies metamorphic sequence. So far, the majority of studies on such *HP/LT* metamorphic rocks focused on their exhumation (e.g. Agard et al., 2009;

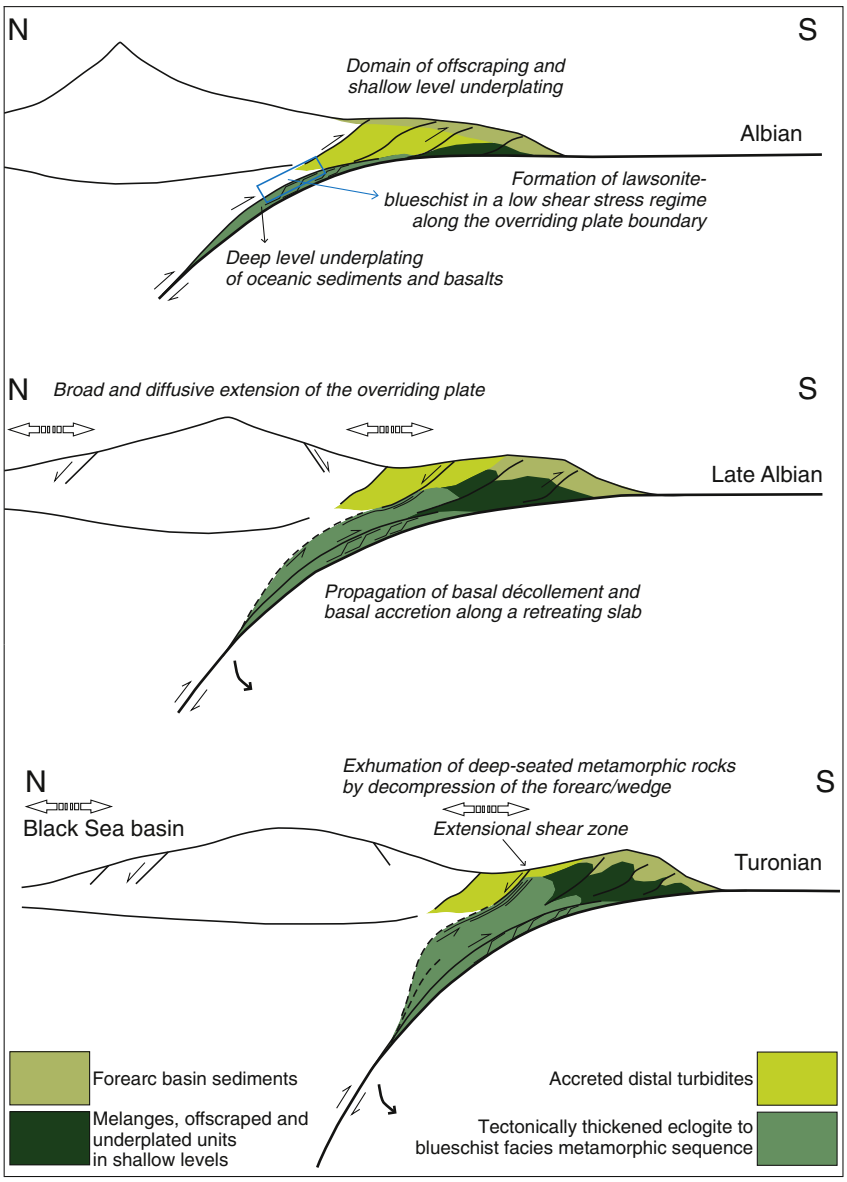

Fig. 14. A model for the tectonic evolution of the Albian–Turonian wedge with a possible tectonic thickening and subsequent exhumation mechanism of the deep seated subduction–accretionary complexes. During the Albian, the wedge dominated by accretion of clastic detritus. Lawsonite blueschists possibly formed during initial stage of Albian subduction characterized by low shear stress. Late Albian to Turonian evolution of the wedge was mainly controlled by slab rollback which creates a necessary space for deep level underplating by décollement propagation. Synchronous extension of the wedge subsequently exhumes the deep-seated metamorphic sequence.

Brun and Brun and Faccenna, 2008; Ganne et al., 2006; Jolivet et al., 2003; Platt, 1993; Sedlock, 1999). However, tectonic thickening of these metamorphic sequences requires considerable amount of space along the plate interface which is generally disregarded. Platt (1986) proposed a general thickening mechanism of the wedge by sediment underplating in a stable subduction zone configuration. Steady state thickening of the wedge is compensated by extension of the wedge (gravity-driven collapse) which also exhumes the H*P*/*LT* metamorphic rocks. Although this mechanism may cause thickening and uplifting of shallow level underplated rocks (e.g. accreted distal turbidites of the Esenler Unit), it is unlikely to solve the space problem along the plate interface for tectonic thickening of deep-seated eclogite to blueschist facies metamorphic sequences (e.g. Domuzdağ Complex).

By interpreting of seismic reflection data, Minelli and Faccenna (2010) reported a post-Messinian basal décollement ramp related to slab rollback in the Calabrian wedge, Italy; which caused frontal thrust propagation and underplating. It is discussed by the same authors that forward propagation of décollement associated with slab rollback can cause crustal thickening (Minelli and Faccenna, 2010). By analogy with the Calabrian wedge, slab rollback also seems the most plausible process that can create a necessary space along plate interface for progressive deep level basal accretion. Thickening of the H*P*/*LT* Domuzdağ Complex is possibly achieved by continuous basal underplating of oceanic basalts and sediments through décollement propagation along the retreating slab (Fig. 14). By extending the wedge, slab rollback also played a major role in subsequent exhumation of the accreted deep-seated Domuzdağ Complex. The extension of the Albian–Turonian accretionary wedge is structurally evidenced by the detachment fault and the footwall micaschists with syn-kinematic albite porphyroblasts. $^{40}Ar/^{39}Ar$ dating on phengites reveals that extensional pervasive shearing occurred in a syn-subduction setting. It is noteworthy that progressive accretion/exhumation should appear with a younging pattern towards the trench. This fits with the 91.8 ± 1.8 Ma age obtained from a chloritoid-micaschist exposed relatively south compared to

100.6 ± 1.3 Ma age in the north. In southern part of the wedge, the Upper Cretaceous (Campanian, Genç et al., 2014) leucite-bearing alkaline volcanic rocks and related turbidites possibly formed above the thinning accretionary wedge related to the continuing slab rollback.

We stress that slab rollback controlled basal décollement propagation and synchronous extension of the wedge might be the most common mechanism of the tectonic thickening and subsequent exhumation of deep-seated H*P*/*LT* subduction–accretionary complexes.

9. Conclusions

Cretaceous H*P*/*LT* metamorphic rocks cover an area of 50 km by 100 km in the Central Pontides and represent accretionary complexes. They comprise both continental and oceanic units resulting pre-collisional accretionary tectonic growth of the southern Laurasian continental margin by ca. 80 km. In the north, the wedge consists of phyllite/metasandstone intercalations with recrystallized limestones, Na-amphibole-bearing metabasites (PT = 7–12 kbar and 400 ± 70 °C) and tectonic slices of serpentinite. The accreted continental metasediments are underlain by H*P*/*LT* metamorphic rocks of oceanic origin along a detachment fault. The oceanic metamorphic sequence comprises tectonically thickened deep-seated eclogite to blueschist facies metabasites and micaschists. In the study area, metabasites are epidote-blueschists locally with garnet (PT = 17 ± 1 kbar and 500 ± 40 °C). Lawsonite-blueschists are exposed as blocks along the detachment fault (PT = 14 ± 2 kbar and 370–440 °C). They are possibly associated with low a shear stress regime during the initial stage of convergence. Age of regional metamorphism is constrained as Albian–Turonian (102–92 Ma) with a southward younging pattern. To the south, the accretionary wedge sequences consist of blueschist and greenschist facies metabasite, marble and volcanogenic metasediment intercalations. $^{40}Ar/^{39}Ar$ phengite dating reveals that this part of the wedge is of Middle Jurassic age partly overprinted during Albian time. Emplacement of Middle Jurassic subduction–accretionary complexes is possibly associated with obliquity of the Albian convergence.

Significant amount of clastic sediment supply from the overriding continental domain into the trench had a primary effect on the enlarging of the Albian accretionary wedge along the Laurasian active margin. Tectonic thickening of the deep-seated oceanic subduction–accretionary complexes was possibly achieved by underplating through propagation of the décollement along a retreating slab which also triggered subsequent syn-subduction exhumation.

Supplementary data to this article can be found online at http://dx.doi.org/10.1016/j.tecto.2016.01.010.

Acknowledgments

We thank Mehmet Ali Oral and Christine Fischer for preparation of the thin sections. Christina Günter is acknowledged for her help during EMPA measurements and Anja Städtke for the XRF analysis. Matthias Konrad-Schmolke is thanked for the fruitful discussions on Theriak-Domino software. We also thank Okan Tüysüz for discussions on the geology of the Central Pontides and Ercan Özcan for paleontological dating of the Maastrichtian limestone. We are grateful to A. H. F. Robertson for his constructive and improving review and editors Evgueni Burov and Rob Govers for further handling the manuscript. İTU and TÜBİTAK research abroad fellowship programs are kindly acknowledged for their supports. Field expenses were funded by İTU Division of Scientific Research Projects for PhD students (project no. 34378). Aral Okay also thanks TÜBA and TÜBİTAK (grant no. 109Y049) for support.

References

Agard, P., Jolivet, L., Goffé, B., 2001. Tectonometamorphic evolution of the Schistes Lustrés complex: implications for the exhumation of HP and UHP rocks in the Western Alps. Bull. Soc. Geol. Fr. 172, 617–636.

Agard, P., Yamato, P., Jolivet, L., Burov, E., 2009. Exhumation of oceanic blueschists and eclogites in subduction zones: timing and mechanisms. Earth-Sci. Rev. 92, 53–79.

Akbayram, K., Okay, A.I., Satır, M., 2013. Early Cretaceous closure of the Intra-Pontide Ocean in western Pontides (northwestern Turkey). J. Geodyn. 65, 38–55.

Altherr, R., Topuz, G., Marschall, H., Zack, T., Ludwig, T., 2004. Evolution of a tourmaline-bearing lawsonite eclogite from the Elekdag area (Central Pontides, N Turkey): evidence for infiltration of slab-derived B-rich fluids during exhumation. Contrib. Mineral. Petrol. 148, 409–425.

Aygül, M., Okay, A.I., Oberhänsli, R., Schmidt, A., Sudo, M., 2015a. Late Cretaceous infant intra-oceanic arc volcanism, the Central Pontides, Turkey: petrogenetic and tectonic implications. J. Asian Earth Sci. 111, 312–327.

Aygül, M., Okay, A.I., Oberhänsli, R., Ziemann, M.A., 2015b. Thermal structure of low-grade accreted Lower Cretaceous distal turbidites, the Central Pontides, Turkey: insights for tectonic thickening of an accretionary wedge. Turkish J. Earth Sci. 24, 461–474.

Aysal, N., Ustaömer, T., Öngen, S., Keskin, M., Köksal, S., Peytcheva, I., Fanning, M., 2012. Origin of the Early–Middle Devonian magmatism in the Sakarya Zone, NW Turkey: geochronology, geochemistry and isotope systematics. J. Asian Earth Sci. 45, 201–222.

Barkurt, M.Y., Bilginer, E., Pehlivan, Ş., Örçen, S., 1990. Geology of the Kastamonu–Ovacık region. MTA Report No: 9079 (in Turkish).

Barr, S.R., Temperley, S., Tarney, J., 1999. Lateral growth of the continental crust through deep level subduction–accretion: a re-evaluation of central Greek Rhodope. Lithos 46, 69–94.

Beck, M.E., 1983. On the mechanism of tectonic transport in zones of oblique subduction. Tectonophysics 93, 1–11.

Boztuğ, D., 1992. Daday–Devrekani Masifi güney kesiminin litostratigrafi birimleri ve tektoniği. Maden Tetkik ve Arama Dergisi 114, pp. 1–20.

Brun, J.P., Faccenna, C., 2008. Exhumation of high-pressure rocks driven by slab rollback. Earth Planet. Sci. Lett. 272, 1–7.

Cawood, P.A., Kröner, A., Collins, W.J., Kusky, T.M., Mooney, W.D., Windley, B.F., 2009. Accretionary orogens through Earth history. In: Cawood, P.A., Kröner, A. (Eds.), Earth Accretionary Systems in Space and Time. Geological Society, London, Special Publications 318, pp. 1–36.

Çelik, Ö.F., Marzoli, A., Marschik, R., Chiaradia, M., Neubauer, F., Öz, İ., 2011. Early–Middle Jurassic intra-oceanic subduction in the İzmir–Ankara–Erzincan Ocean, Northern Turkey. Tectonophysics 509, 120–134.

Chen, F., Siebel, W., Satır, M., Terzioğlu, N., Saka, K., 2002. Geochronology of the Karadere basement (NW Turkey) and implications for the geological evolution of the İstanbul Zone. Int. J. Earth Sci. 91, 469–481.

Cloos, M., 1993. Lithospheric buoyancy and collisional orogenesis: subduction of oceanic plateaus, continental margins, island arcs, spreading ridges, and seamounts. Geol. Soc. Am. Bull. 105, 715–737.

de Capitani, C., Brown, T.H., 1987. The computation of chemical equilibrium in complex systems containing non-ideal solutions. Geochim. Cosmochim. Acta 51, 2639–2652.

de Capitani, C., Petrakakis, K., 2010. The computation of equilibrium assemblage diagrams with Theriak/Domino software. Am. Mineral. 95, 1006–1016.

Dean, W.T., Monod, O., Rickards, R.B., Demir, O., Bultynck, P., 2000. Lower Palaeozoic stratigraphy and palaeontology, Karadere–Zirze area, Pontus Mountains, northern Turkey. Geol. Mag. 137, 555–582.

Dickinson, W.R., 2008. Accretionary Mesozoic–Cenozoic expansion of the Cordilleran continental margin in California and adjacent Oregon. Geosphere 4, 329–353.

Dodson, M.H., 1973. Closure temperature in cooling geochronological and petrological systems. Contrib. Mineral. Petrol. 40, 259–274.

Fitch, T.J., 1972. Plate convergence, transcurrent faults, and internal deformation adjacent to Southeast Asia and the western Pacific. J. Geophys. Res. 77, 4432–4460.

Foster, D.A., Gray, D.R., 2000. Evolution and structure of the Lachlan Fold Belt (Orogen) of Eastern Australia. Annu. Rev. Earth Planet. Sci. 28, 47–80.

Fuis, G.S., et al., 2008. Trans-Alaska crustal transect and continental evolution involving subduction underplating and synchronous foreland thrusting. Geology 36, 267–270.

Ganne, J., Marquer, D., Rosenbaum, G., Bertrand, J–.M., Fudral, S., 2006. Partitioning of deformation within a subduction channel during exhumation of high-pressure rocks: a case study from the Western Alps. J. Struct. Geol. 28, 1193–1207.

Genç, Ş.C., Tüysüz, O., 2010. Tectonic setting of the Jurassic bimodal magmatism in the Sakarya Zone (Central and Western Pontides), Northern Turkey: a geochemical and isotopic approach. Lithos 118, 95–111.

Genç, Ş.C., Gülmez, F., Karacık, Z., Tüysüz, O., Prelevic, D., Roden, M.F., Hames, W.E., Billor, M.Z., 2014. Subduction-related high- to ultrahigh-potassic rocks of the Ankara–Erzincan Suture Belt of Turkey: a geochemical and isotopic approach to source and petrogenesis. Geophys. Res. Abstr. 16 (EGU2014-14565-1).

Göçmengil, G., Altıntaş, İ.E., Topuz, G., Çelik, Ö.F., Özkan, M., 2013. Diverse tectonic settings of formation of the metaigneous rocks in the Jurassic metamorphic accretionary complexes (Refahiye, NE Turkey) and their geodynamic implications. Geodin. Acta http://dx.doi.org/10.1080/09853111.2013.858946.

Göncüoglu, M.C., Marroni, M., Pandolfi, L., Ellero, A., Ottria, G., Catanzariti, R., Tekin, U.K., Sayit, K., 2014. The Arkot Dağ Melange in Araç area, central Turkey: evidence of its origin within the geodynamic evolution of the Intra-Pontide suture zone. J. Asian Earth Sci. 85, 117–139.

Gülmez, F., Genç, Ş.C., Prelevic, D., 2014. Petrology and geochemistry of late Cretaceous lamprophyric rocks from North Anatolian Ophiolitic Melange—Turkey. Geophys. Res. Abstr. 16 (EGU2014-14914).

Halama, R., Konrad–Schmolke, M., Sudo, M., Marschall, H.R., Wiedenbeck, M., 2014. Effects of fluid–rock interaction on $^{40}Ar/^{39}Ar$ geochronology in high-pressure rocks (Sesia-Lanzo Zone, Western Alps). Geochim. Cosmochim. Acta 126, 475–494.

Harrison, T.M., Célérier, J., Aikman, A.B., Hermann, J., Heizler, M.T., 2009. Diffusion of ^{40}Ar in muscovite. Geochim. Cosmochim. Acta 73, 1039–1051.

Hippolyte, J.C., Müller, C., Kaymakçı, N., Sangu, E., Sosson, M., Kaymakçı, N., Stephenson, R.A., Bergerat, F., 2010. Dating of the Black Sea Basin: new nannoplankton ages from its inverted margin in the Central Pontides (Turkey). In: Starostenko, V. (Ed.),

Sedimentary Basin Tectonics From the Black Sea and Caucasus to the Arabian Platform. Geological Society of London, Special Publication 340, pp. 113–136.
Holland, T., Powell, R., 1998. An internally consistent thermodynamic data set for phases of petrological interest. J. Metamorph. Geol. 16, 309–343.
Isozaki, Y., 1996. Anatomy and genesis of a subduction-related orogen: a new view of geotectonic subdivision and evolution of the Japanese Islands. Island Arc 5, 289–320.
Jarrard, R.D., 1986. Terrane motion by strike-slip faulting of forearc slivers. Geology 14, 780–783.
Jolivet, L., Faccenna, C., Goffé, B., Burov, E., Agard, P., 2003. Subduction tectonics and exhumation of high-pressure metamorphic rocks in the Mediterranean orogens. Am. J. Sci. 303, 353–409.
Karig, D.E., Sharman, G.F., 1975. Subduction and accretion in trenches. Geol. Soc. Am. Bull. 86, 377–389.
Kimura, G., Maruyama, S., Isozaki, Y., Terabayashi, M., 1996. Well-preserved underplating structure of the jadeitized Franciscan complex, Pacheco Pass, California. Geology 24, 75–78.
Marroni, M., Frassi, C., Göncüoglu, M.C., Di Vincenzo, G., Pandolfi, L., Rebay, G., Ellero, A., Ottria, G., 2014. Late Jurassic amphibolite-facies metamorphism in the Intra-Pontide Suture Zone (Turkey): an eastward extension of the Vardar Ocean from the Balkans into Anatolia? J. Geol. Soc. http://dx.doi.org/10.1144/jgs2013–104.
Maruyama, S., 1997. Pacific-type orogeny revisited: Miyashiro-type orogeny proposed. Island Arc 6, 91–120.
McCaffrey, R., 1992. Oblique plate convergence, slip vectors, and forearc deformation. J. Geophys. Res. 97, 8905–8915.
Meijers, M.J.M., Nuretdin, K., van Hinsbergen, D.J.J., Langereis, C.G., Stephenson, R.A., Hippolyte, J–.C., 2010. Late Cretaceous to Paleocene oroclinal bending in the central Pontides (Turkey). Tectonics 29, TC4016. http://dx.doi.org/10.1029/2009TC002620.
Minelli, L., Faccenna, C., 2010. Evolution of the Calabrian accretionary wedge (central Mediterranean). Tectonics 29, TC4004. http://dx.doi.org/10.1029/2009TC002562.
Moore, J.C., Biju–Duval, B., Bergen, J.A., Blackington, G., Claypool, G.E., Dowan, D.S., Duennebier, F., Guerra, R.T., Hemleben, C.H.J., Hussong, D., Marlow, M.S., Natland, J.H., Pudsey, C.J., Renz, G.W., Tardy, M., Willis, M.E., Wilson, D., Wright, A.A., 1982. Offscraping and underthrusting of sediment at the deformation front of the Barbados Ridge: Deep Sea Drilling Project leg 78 A. Geol. Soc. Am. Bull. 93, 1065–1077.
Moore, J.C., Diebold, J., Fisher, M.A., Sample, J., Brocher, T., Talwani, M., Ewing, J., von Huene, R., Rowe, C., Stone, D., Stevens, C., Sawyer, D., 1991. EDGE deep seismic reflection transect of the eastern Aleutian arc–trench layered lower crust reveals underplating and continental growth. Geology 19, 420–424.
Nzegge, O.M., Satır, M., Siebel, W., Taubald, H., 2006. Geochemical and isotopic constraints on the genesis of the Late Palaeozoic Deliktas, and Sivrikaya granites from the Kastamonu granitoid belt (Central Pontides, Turkey). Neues JahrBuch für Mineralogie 183, pp. 27–40.
Okay, A.I., 1989. Tectonic units and sutures in the Pontides, Northern Turkey. In: A.M.C., Şengör (Ed.), Tectonic Evolution of the Tethyan Region. Kluwer academic publishers, pp. 109–116.
Okay, A.I., 2000. Was the Late Triassic orogeny in Turkey caused by the collision of an oceanic plateau? In: Bozkurt, E., Winchester, J.A., Piper, J.D.A. (Eds.), Tectonics and Magmatism in Turkey and Surrounding Area 173. Geological Society of London, Special Publication, pp. 25–41
Okay, A.I., Monié, P., 1997. Early Mesozoic subduction in the Eastern Mediterranean: evidence from Triassic eclogite in northwest Turkey. Geology 25, 595–598.
Okay, A.I., Tüysüz, O., 1999. Tethyan sutures of northern Turkey. In: Durand, B., Jolivet, L., Horvath, F., Seranne, M. (Eds.), The Mediterranean Basins: Tertiary Extension Within the Alpine Orogen 156. Geological Society, London, Special Publication, pp. 475–515.
Okay, A.I., Şengör, A.M.C., Görür, N., 1994. Kinematic history of the opening of the Black Sea and its effect on the surrounding regions. Geology 22, 267–270.
Okay, A.I., Satır, M., Maluski, H., Siyako, M., Monie, P., Metzger, R., Akyüz, S., 1996. Palaeo- and Neo-Tethyan events in northwest Turkey. In: Harrison, M. (Ed.), Yin, E. Cambridge University Press, Tectonics of Asia, pp. 420–441.
Okay, A.I., Monod, O., Monie, P., 2002. Triassic blueschists and eclogites from northwest Turkey: vestiges of the Paleo-Tethyan Subduction. Lithos 64, 155–178.
Okay, A.I., Tüysüz, O., Satır, M., Özkan–Altıner, S., Altıner, D., Sherlock, S., Eren, R.H., 2006a. Cretaceous and Triassic subduction–accretion, HP/LT metamorphism and continental growth in the Central Pontides, Turkey. Geol. Soc. Am. Bull. 118, 1247–1269.
Okay, A.I., Satır, M., Siebel, W., 2006b. Pre-Alpide Palaezoic and Mesozoic orogenic events in the Eastern Mediterranean region. In: Gee, D.G., Stephenson, R.A. (Eds.), European Lithosphere Dynamics. Geological Society, London, Memoirs 32, pp. 389–405.
Okay, A.I., Sunal, G., Sherlock, S., Altıner, D., Tüysüz, O., Kylander–Clark, A.R.C., Aygül, M., 2013. Early Cretaceous sedimentation and orogeny on the active margin of Eurasia: Southern Central Pontides, Turkey. Tectonics 32, 1247–1271.
Okay, A.I., Sunal, G., Tüysüz, O., Sherlock, S., Keskin, M., Kylander–Clark, A.R.C., 2014. Low-pressure–high-temperature metamorphism during extension in a Jurassic magmatic arc, Central Pontides, Turkey. J. Metamorph. Geol. 32, 49–69.
Okay, A.I., Altıner, D., Kılıç, A.M., 2015. Triassic limestone, turbidites and serpentinite—the Cimmeride orogeny in the Central Pontides. Geol. Mag. http://dx.doi.org/10.1017/S0016756814000429.
Otsuki, M., Banno, S., 1990. Prograde and retrograde metamorphism of hematite-bearing basic schists in the Sanbagawa belt in central Shikoku. J. Metamorph. Geol. 8, 425–439.
Özcan, E., Less, G., Kertesz, B., 2007. Late Ypresian to middle Lutetian orthophragminid record from central and northern Turkey: taxonomy and remarks on zonal scheme. Turk. J. Earth Sci. 16, 281–318.
Peacock, S.M., 1992. Blueschist-facies metamorphism, shear heating, and P–T–t paths in subduction shear zones. J. Geophys. Res. 97, 17693–17707.
Peacock, S.M., 1996. Thermal and petrologic structure of subduction zones. In: Bebout, G.E., Scholl, D.W., Kirby, S.H., Platt, J.P. (Eds.), Subduction Top to Bottom. American Geophysical Union, Washington, D. C. http://dx.doi.org/10.1029/GM096p0119.
Pickett, E.A., Robertson, A.H.F., 2004. Significance of the volcanogenic Nilüfer Unit and related components of the Triassic Karakaya Complex for Tethyan subduction/accretion processes in NW Turkey. Turk. J. Earth Sci. 13, 97–144.
Platt, J.P., 1986. Dynamics of orogenic wedges and the uplift of high-pressure metamorphic rocks. Geol. Soc. Am. Bull. 97, 1037–1053.
Platt, J.P., 1993. Exhumation of high-pressure rocks: a review of concepts and processes. Terra Nova 5, 119–133.
Platt, J.P., Leggett, J.K., Young, J., Raza, H., Alam, S., 1985. Large scale sediment underplating in the Makran accretionary prism, southwest Pakistan. Geology 13, 507–511.
Powell, R., Holland, T., 1988. An internally consistent thermodynamic dataset with uncertainties and correlations: 3. Application methods, worked examples and a computer program. J. Metamorph. Geol. 6, 173–204.
Rice, S.P., Robertson, A.H.F., Ustaömer, T., 2006. Late Cretaceous–early Cenozoic tectonic evolution of the Eurasian active margin in the Central and Eastern Pontides, northern Turkey. In: Robertson, A.H.F., Mountrakis, D. (Eds.), Tectonic Development of the Eastern Mediterranean Region. Geological Society, London, Special Publications 260, pp. 413–445.
Robertson, A.H.F., Ustaömer, T., 2004. Tectonic evolution of the Intra-Pontide suture zone in the Armutlu Peninsula NW Turkey. Tectonophysics 381, 175–209.
Robertson, A.H.F., Ustaömer, T., 2012. Testing alternative tectono-stratigraphic interpretations of the Late Palaeozoic–Early Mesozoic Karakaya Complex in NW Turkey: support for an accretionary origin related to northward subduction of Palaeotethys. Turkish J. Earth Sci. 21, 961–1007.
Sample, J.C., Fisher, D.M., 1986. Duplex accretion and underplating in an ancient accretionary complex, Kodiak Islands, Alaska. Geology 14, 160–163.
Schiffman, P., Day, H.W., 1999. Petrological methods for the study of very low-grade metabasites. In: Frey, M., Robinson, D. (Eds.), Low-grade Metamorphism. Blackwell Science Ltd., Oxford, London (313 pp.).
Schumacher, J.C., 1997. The estimation of the proportion of ferric iron in the electron-microprobe analysis of amphiboles. Can. Mineral. 35, 238–246.
Sedlock, R.L., 1999. Evaluation of exhumation mechanisms for coherent blueschists in western Baja California, Mexico. In: Ring, U., Brandon, M.T., Lister, G.S., Willett, S.D. (Eds.), Exhumation Processes: Normal Faulting, Ductile Flow and Erosion. Geological Society, London, Special Publications 154, pp. 29–54.
Seely, D.R., Vail, P.R., Walton, G.G., 1974. Trench slope model. In: Burk, C.A., Drake, C.L. (Eds.), The Geology of the Continental Margins. Springer, New York, pp. 249–260.
Şengör, A.M.C., Natal'in, B.A., 1996. Turkic-type orogeny and its role in the making of the continental crust. Annu. Rev. Earth Planet. Sci. 24, 263–337.
Şengör, A.M.C., Yilmaz, Y., 1981. Tethyan evolution of Turkey: a plate tectonic approach. Tectonophysics 75, 181–241.
Şengör, A.M.C., Natal'in, B.A., Burtman, V.S., 1993. Evolution of the Altaid tectonic collage and Palaeozoic crustal growth in Eurasia. Nature 364, 299–307.
Spaggiari, C.V., Gray, D.R., Foster, D.A., 2002. Blueschist metamorphism during accretion in the Lachlan Orogen, south-eastern Australia. J. Metamorph. Geol. 20, 711–726.
Sunal, G., 2012. Devonian magmatism in the western Sakarya Zone, Karacabey region, NW Turkey. Geodin. Acta 25, 183–201.
Takasu, A., Wallis, S.R., Banno, S., Dallmeyer, R.D., 1994. Evolution of the Sambagawa metamorphic belt, Japan. Lithos 33, 119–133.
Topuz, G., Altherr, R., Kalt, A., Satır, M., Werner, O., Schwartz, W.H., 2004. Aluminous granulites from the Pulur Complex, NE Turkey: a case of partial melting, efficient melt extraction and crystallisation. Lithos 72, 183–207.
Topuz, G., Altherr, R., Schwartz, W.H., Dokuz, A., Meyer, H–.P., 2007. Variscan amphibolites-facies rocks from the Kurtoğlu metamorphic complex (Gümüşhane area, Eastern Pontides, Turkey). Int. J. Earth Sci. 96, 861–873.
Topuz, G., Göçmengil, G., Rolland, Y., Çelik, Ö.F., Zack, T., Schmitt, A.K., 2012. Jurassic accretionary complex and ophiolite from northeast Turkey: no evidence for the Cimmerian continental ribbon. Geology 41, 255–258.
Topuz, G., Okay, A.İ., Altherr, R., Schwarz, W.H., Sunal, G., Altinkaynak, L., 2014. Triassic warm subduction in northeast Turkey: evidence from the Ağvanis metamorphic rocks. Island Arc. http://dx.doi.org/10.1111/iar.12068.
Tsujimori, T., Matsumoto, K., Wakabayashi, J., Liou, J.G., 2006a. Franciscan eclogite revisited: reevaluation of the P–T evolution of tectonic blocks from Tiburon Peninsula, California, U.S.A. Mineral. Petrol. 88, 243–267.
Tsujimori, T., Sisson, V.B., Liou, J.G., Harlow, G.E., Sorensen, S.S., 2006b. Very-low temperature record of the subduction process: a review of worldwide lawsonite eclogites. Lithos 92, 609–624.
Tüysüz, O., 1990. Tectonic evolution of a part of the Tethyside orogenic collage: the Kargı Massif, northern Turkey. Tectonics 9, 141–160.
Tüysüz, O., 1999. Geology of the Cretaceous sedimentary basins of the Western Pontides. Geol. J. 34, 75–93.
Tüysüz, O., Tekin, U.K., 2007. Timing of imbrication of an active continental margin facing the northern branch of Neotethys, Kargı Massif, northern Turkey. Cretac. Res. 28, 754–764.
Tüysüz, O., Yılmaz, İ.Ö., Švábenická, L., Kirici, S., 2012. The Unaz Formation: a key unit in the western Black Sea Region, N Turkey. Turkish J. Earth Sci. 21, 1009–1028.
Tüysüz, O., Melinte–Dobrinescu, M.C., Yılmaz, İ.Ö., Kirici, S., Švábenická, L., Skupien, P., 2015. The Kapanboğazı formation: a key unit for understanding Late Cretaceous evolution of the Pontides, N Turkey. Palaeogeogr. Palaeoclimatol. Palaeoecol. http://dx.doi.org/10.1016/j.palaeo.2015.06.028
Uğuz, M.F., Sevin, M., Duru, M., 2002. Geological Map of Turkey. 1: 500.000 Scaled Sinop Sheet. Maden Tetkik ve Arama Genel Müdürlüğü, Ankara.
Ujiee, K., 1997. Off-scraping accretionary process under the subduction of young oceanic crust: the Shimanto Belt of Okinawa Island, Ryukyu Arc. Tectonics 16, 305–322.
Ustaömer, T., Robertson, A.H.F., 1993. A Late Paleozoic–Early Mesozoic marginal basin along the active southern continental margin of Eurasia: evidence from the Central Pontides (Turkey) and adjacent regions. Geol. J. 28, 219–238.

Ustaömer, T., Robertson, A.H.F., 1994. Late Paleozoic marginal basin and subduction–accretion: the Paleotethyan Küre Cromplex, Central Pontides, northern Turkey. J. Geol. Soc. 151, 291–305.
Ustaömer, T., Robertson, A.H.F., 1997. Tectonic-sedimentary evolution of the North-Tethyan margin in the Central Pontides of northern Turkey. In: Robinson, A.G. (Ed.), Regional and Petroleum Geology of the Black Sea and Surrounding Region. American Association of Petroleum Geologists, Memoir 68, pp. 255–290.
Ustaömer, T., Robertson, A.H.F., 1999. Geochemical evidence used to test alternative plate tectonic models for pre-Upper Jurassic (Palaeotethyan) units in the Central Pontides, N Turkey. Geol. J. 34, 25–53.
Ustaömer, P.A., Rogers, G., 1999. The Bolu Massif: remnant of a pre-Early Ordovician active margin in the west Pontides, northern Turkey. Geol. Mag. 136, 579–592.
Ustaömer, P.A., Mundil, R., Renne, P.R., 2005. U/Pb and Pb/Pb zircon ages for arc-related intrusions of the Bolu Massif (W Pontides, NW Turkey): evidence for Late Precambrian (Cadomian) age. Terra Nova 17, 215–223.
van den Beukel, J., Wortel, R., 1987. Temperatures and shear stresses in the upper part of a subduction zone. Geophys. Res. Lett. 14, 1057–1060.
Villa, I.M., 1998. Isotopic closure. Terra Nova 10, 42–47.
Whitney, D.L., Davis, P.B., 2006. Why is lawsonite eclogite so rare? Metamorphism and preservation of lawsonite eclogite, Sivrihisar, Turkey. Geology 34, 473–476.
Wilke, F.D.H., O'Brien, P.J., Gerdes, A., Timmerman, M.J., Sudo, M., Khan, M.A., 2010. The multistage exhumation history of the Kaghan Valley UHP series, NW Himalaya, Pakistan from U–Pb and $^{40}Ar/^{39}Ar$ ages. Eur. J. Mineral. 22, 703–719.
Yiğitbaş, E., Kerrich, R., Yılmaz, Y., Elmas, A., Xie, Q., 2004. Characteristics and geochemistry of Precambrian ophiolites and related volcanics from the İstanbul–Zonguldak Unit, Northwestern Anatolia, Turkey: following the missing chain of the Precambrian South European suture zone to the east. Precambrian Res. 132, 179–206.
Yılmaz, O., Boztuğ, D., 1986. Kastamonu granitoid belt of northern Turkey: first arc plutonism product related to the subduction of the Paleo-Tethys. Geology 14, 179–183.
Yılmaz, Y., Şengör, A.M.C., 1985. Paleo-Tethyan ophiolites in northern Turkey: petrology and tectonic setting. In: Desmons, J. (Ed.), Ophiolites Through Times, Conf. Proceed. vol. 10(2–3), pp. 485–504.
Yılmaz, Y., Tüysüz, O., Yiğitbaş, E., Genç, Ş.C., Şengör, A.M.C., 1997. Geology and tectonic evolution of the Pontides. In: Robinson, A.G. (Ed.), Regional and Petroleum Geology of the Black Sea and Surrounding Region. American Association of Petroleum Geologists, Memoir 68, pp. 183–226.
Zack, T., Rivers, T., Brumm, R., Kronz, A., 2004. Cold subduction of oceanic crust: implications from a lawsonite eclogite from the Dominican Republic. Eur. J. Mineral. 16, 909–916.